AD-A177 112 MOVING FINITE ELEMENTS IN 2-D -- FLUID DYNAMICS APPLICATIONS(U) SCIENCE APPLICATIONS INTERNATIONAL CORP PLEASANTON CA R J GELINAS 30 JAN 84 SAI-83/1057 1/1

UNCLASSIFIED DNA-TR-84-60 DNA001-82-C-0223 F/G 20/4 NL

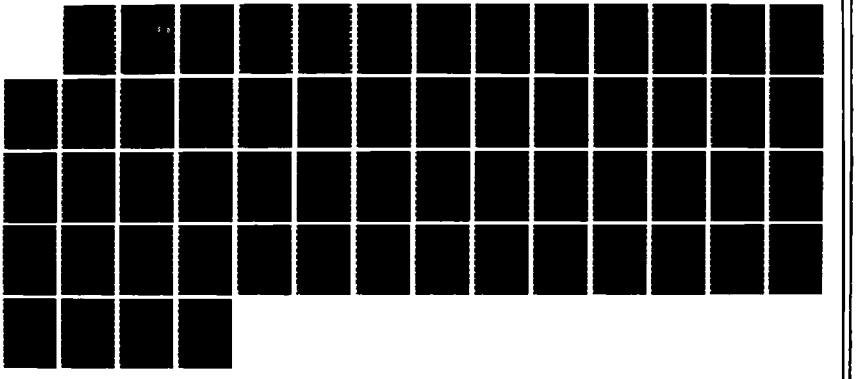

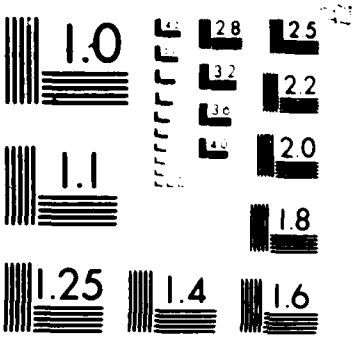
1.0
1.1
1.25
1.4
1.6
1.8
2.0
2.2
2.5
2.8
3.2
3.6
4.0

(12)

DNA-TR-84-60

MOVING FINITE ELEMENTS IN 2-D

Fluid Dynamics Applications

Robert J. Gelinas
Science Applications International Corporation
3015 Hopyard Road
Suite M
Pleasanton, CA 94566

30 January 1984

Technical Report

CONTRACT No. DNA 001-82-C-0223

Approved for public release;
distribution is unlimited.

THIS WORK WAS SPONSORED BY THE DEFENSE NUCLEAR AGENCY
UNDER RDT&E RMSS CODE B344082466 Y99QAXSG00048 H2590D.

Prepared for
Director
DEFENSE NUCLEAR AGENCY
Washington, DC 20305-1000

Destroy this report when it is no longer needed. Do not return to sender.

PLEASE NOTIFY THE DEFENSE NUCLEAR AGENCY, ATTN: STTI, WASHINGTON, DC 20305-1000, IF YOUR ADDRESS IS INCORRECT, IF YOU WISH IT DELETED FROM THE DISTRIBUTION LIST, OR IF THE ADDRESSEE IS NO LONGER EMPLOYED BY YOUR ORGANIZATION.

DISTRIBUTION LIST UPDATE

This mailer is provided to enable DNA to maintain current distribution lists for reports. We would appreciate your providing the requested information.

☐ Add the individual listed to your distribution list.

☐ Delete the cited organization/individual.

☐ Change of address.

NAME: _____

ORGANIZATION: _____

OLD ADDRESS	CURRENT ADDRESS
_____	_____
_____	_____
_____	_____

TELEPHONE NUMBER: ( ) _____

SUBJECT AREA(s) OF INTEREST:

_____	_____
_____	_____
_____	_____

DNA OR OTHER GOVERNMENT CONTRACT NUMBER: _____

CERTIFICATION OF NEED-TO-KNOW BY GOVERNMENT SPONSOR (if other than DNA):

SPONSORING ORGANIZATION: _____

CONTRACTING OFFICER OR REPRESENTATIVE: _____

SIGNATURE: _____

Director
Defense Nuclear Agency
ATTN: STTI
Washington, DC 20305-1000

Director
Defense Nuclear Agency
ATTN: STTI
Washington, DC 20305-1000

UNCLASSIFIED
SECURITY CLASSIFICATION OF THIS PAGE

AD-A177112

REPORT DOCUMENTATION PAGE

Form Approved
OMB No. 0704-0188
Exp. Date: Jun 30, 1986

1a REPORT SECURITY CLASSIFICATION UNCLASSIFIED	1b RESTRICTIVE MARKINGS
2a SECURITY CLASSIFICATION AUTHORITY N/A since Unclassified	3 DISTRIBUTION/AVAILABILITY OF REPORT Approved for public release; distribution is unlimited.
2b DECLASSIFICATION/DOWNGRADING SCHEDULE N/A since Unclassified	
4 PERFORMING ORGANIZATION REPORT NUMBER(S) SAI-83/1057	5 MONITORING ORGANIZATION REPORT NUMBER(S) DNA-TR-84-60
6a NAME OF PERFORMING ORGANIZATION Science Applications International Corporation 6b OFFICE SYMBOL (If applicable)	7a NAME OF MONITORING ORGANIZATION Director Defense Nuclear Agency
6c ADDRESS (City, State, and ZIP Code) 3015 Hopyard Road, Suite M Pleasanton, CA 94566	7b ADDRESS (City, State, and ZIP Code) Washington, DC 20305-1000
8a NAME OF FUNDING/SPONSORING ORGANIZATION 8b OFFICE SYMBOL (If applicable)	9 PROCUREMENT INSTRUMENT IDENTIFICATION NUMBER DNA 001-82-C-0223
8c ADDRESS (City, State, and ZIP Code)	10 SOURCE OF FUNDING NUMBERS PROGRAM ELEMENT NO: 62715H; PROJECT NO: Y99QAXS; TASK NO: G; WORK UNIT ACCESSION NO: DH006211

11 TITLE (Include Security Classification)
MOVING FINITE ELEMENTS IN 2-D
Fluid Dynamics Applications

12 PERSONAL AUTHOR(S)
Gelinas, Robert J.

13a TYPE OF REPORT	13b TIME COVERED	14 DATE OF REPORT (Year, Month, Day)	15 PAGE COUNT
Technical	FROM 820707 TO 840130	840130	58

16 SUPPLEMENTARY NOTATION
This work was sponsored by the Defense Nuclear Agency under RDT&E RMSS Code B344082466 Y99QAXSG00048 H2590D.

17 COSATI CODES			18 SUBJECT TERMS (Continue on reverse if necessary and identify by block number)
FIELD	GROUP	SUB-GROUP	
20	4		Moving Nodes, Implicit Solutions, Finite Elements, Partial Differential Equation, Viscous Dissipation, Navier-Stokes Equations
12	1		

19 ABSTRACT (Continue on reverse if necessary and identify by block number)

This report summarizes progress in the first full year's research on the feasibility of using the moving finite element (MFE) method in 2-D for the study of shock boundary layer interactions. It is found that highly local physical dissipation processes in regions of large gradients can be sensitive determinates of macroscopic flow properties. The MFE method continues to show promise for resolving such physical effects, while suppressing anomolous or numerical diffusion effects, over highly disparate physical scales. Recommendations are given for improving the MFE method for further reduction to practice for airblast applications.

20 DISTRIBUTION/AVAILABILITY OF ABSTRACT ☐ UNCLASSIFIED/UNLIMITED ☒ SAME AS RPT ☐ DTIC USERS	21 ABSTRACT SECURITY CLASSIFICATION UNCLASSIFIED
22a NAME OF RESPONSIBLE INDIVIDUAL Betty L. Fox	22b TELEPHONE (Include Area Code) (202) 325-7042 22c OFFICE SYMBOL DNA/STTI

DD FORM 1473, 84 MAR 83 APR edition may be used until exhausted
All other editions are obsolete

SECURITY CLASSIFICATION OF THIS PAGE
UNCLASSIFIED

18. SUBJECT TERMS (Continued)

Shock-Boundary Layer Interactions

TABLE OF CONTENTS

LIST OF ILLUSTRATIONS

LIST OF ILLUSTRATIONS (continued)

LIST OF ILLUSTRATIONS (continued)

SECTION 1
INTRODUCTION

It is well known in aerodynamics that shockwave-boundary layer interactions are dependent upon local viscous dissipation and thermal conduction processes for the distribution of internal and kinetic energies. This dependence can in many applications be a sensitive determinate of macroscopic flow properties. In airblast applications it is clear that, in both clear and dusty atmospheres, irregular shock reflection processes evolve from such local shock interactions with boundary layers and possibly with other internal shear layer regimes. These types of shock-boundary/shear layer processes impose severe demands upon computer codes which attempt to calculate airblast effects.

It is certainly important in studies of shock-boundary layer interactions to either eliminate or suppress to extremely low levels the purely numerical dissipation effects which are present in existing hydrodynamics codes. This is both difficult and ambiguous in inviscid PDE's because: (i) they contain no physical dissipation operators which are present in real-world shocks and boundary layers, and (ii) the codes which solve such PDE's thus generate only numerical dissipation in those critical interaction regimes of the PDE solutions. It follows that the most reliable computations of the essential physics of shock-boundary layer interaction processes must first include the physical dissipation operators of the full Navier-Stokes equations and then use optimally distributed grid densities which can accurately resolve the actual physical dissipation processes and eliminate the numerical dissipation processes.

It appears that neither of these last-mentioned factors have been accommodated adequately in existing airblast codes; and, for fundamental physical and mathematical reasons there is cause for concern that these factors may never be handled adequately by extended versions of most existing airblast codes.

As a possible alternative, the Moving Finite Element (MFE) method, which was discovered by Professor Keith Miller in the mid-1970's has shown some promise of adequately dealing with the combined physical and numerical

requirements of irregular shock reflection processes. It has so far been shown in 1-D calculations that the MFE method successfully resolves shock-boundary/shear layer interactions according to the full Navier-Stokes equations. In these 1-D results, the essential physical dissipation processes were resolved accurately over highly disparate spatial and temporal scales with a minimal number of optimally distributed moving grid nodes. But despite the promise shown in these early 1-D results, it was by no means certain that the MFE method would also extend effectively to 2-D for the resolution of irregular shock reflection processes.

In view of these circumstances, the present research and development effort was undertaken by DNA as a two-year project to determine the feasibility of applying the MFE method to airblast problems in 2-D and, if warranted, to develop a 2-D MFE production code for airblast applications. This report summarizes the results of the first full year's effort which has been devoted to the following work statement tasks:

1. Survey and select sample problems which test the effectiveness of the MFE method and alternative PDE solution methods for resolving blast wave effects, including shock reflections and interactions in 2-D, with particular attention to the resolution of physical vs. numerical dissipation effects.

2. Develop new coding of the gas dynamics operators in 2-D for MFE applications to hydrodynamics.

3. Test alternative node control strategies for 2-D hydrodynamics applications.

4. Test and implement more efficient matrix solution methods in the interest of computational economy in the MFE hydrodynamics code.

These tasks have been carried out successfully as will be described in the three main report sections which follow sequentially under the headings of MAIN TEXT, CONCLUSIONS, and RECOMMENDATIONS.

SECTION 2
BACKGROUND

The problem of primary concern is the accurate calculation of HOB overpressures as a function of range, altitude, and time for various field conditions. Despite numerous ongoing efforts to calculate such HOB data by alternative computational approaches, significant discrepancies remain between the various calculations in comparisons against each other and in comparisons against experimental data. While debate and analysis of these respective discrepancies continue, there remains the gnawing possibility that certain essential physics processes in regions of large gradients which drive the real-world systems are neither included nor otherwise resolved adequately in existing code calculations. It is also possible that some of the essential driving physical processes are not measured directly or otherwise distinguished by detailed cause-and-effect experiments in field measurements.

This project thus attempts to obtain accurate MFE solutions of the full Navier-Stokes equations for irregular shock reflection processes. It appears that the highly detailed reflected shock data obtained in the laboratory by Glass and co-workers[1] provides the most appropriate data base for benchmarking codes which would attempt to calculate shock-boundary/shear layer interactions. We concur with the (paraphrased) view expressed by Glass that codes which are to be used to calculate HOB effects in non-ideal atmospheres should certainly be able to solve accurately, as a first pre-requisite, those physical processes which account for the observed isopycnic data in carefully controlled laboratory experiments of regular and irregular shock reflections in idealized atmospheres. We therefore consider the calculation of Glass's shock reflection data as an essential set of standard shock test examples for DNA airblast problems.

2.1 MATHEMATICAL BACKGROUND OF THE MFE METHOD.

In order to present a coherent report of work to the broadest range of readers, we present here a brief mathematical sketch of the MFE method. Consider a general system of partial differential equations (PDE's), $\dot{U} = L(U)$ or

$$\dot{u}_1 = L_1(U) \quad , \qquad (1)$$

$$\dot{u}_N = L_N(U) \quad .$$

Using piecewise linear approxminants of $u_1 \ldots u_N$,* which are of the form $u = mx + ny + p$, on a hexagonally connected triangular mesh (Figures 1-3), application of the chain rule to the differentiation of u_k gives:

$$\dot{u}_k = \sum_j \dot{a}k_j \alpha k^j + \dot{x}_j \beta k^j + \dot{y}_j \gamma k^j \quad , \text{ where} \tag{2a}$$

$$\alpha k^j = \alpha^j = \frac{\partial u_k}{\partial a k_j} \; ; \; \beta k^j = \frac{\partial u_k}{\partial x_j} \; ; \; \gamma k^j = \frac{\partial u_k}{\partial y_j} \quad . \tag{2b}$$

The key aspect of the MFE method lies in the rigorous retention of the nodal motion terms involving $\dot{x}$ and $\dot{y}$. In most conventional PDE solution methods, the nodal motion terms are either set to zero (fixed nodes) or allowed to assume some arbitrary selected values (e.g., mean fluid velocities in Lagrangian codes).

Alternatively, the MFE method uses a very fundamental criterion for the evaluation of grid node motions ($\dot{x}$ and $\dot{y}$) at every time step. That is, the basic MFE method is formulated by requiring that all of the time derivatives $\dot{a}l_j, \ldots, \dot{a}N_j, \dot{x}_j, \dot{y}_j$ be found at each instant in such a way as to minimize the L^2 norm of the PDE residual, $|| \dot{U} - L(U) ||$. This has been found to minimize PDE solution errors and to dramatically reduce the number of grid nodes. In order to handle the degeneracies which can sometimes occur in such a parametrization of PDE solutions, regularization techniques are applied. That is, the more general function,

$$\psi \equiv w_1^2 || \dot{u}_1 - L_1(U) ||^2 + \ldots w_N^2 || \dot{u}_N - L_N(U) ||^2$$

$$+ \sum_{\substack{\text{triangle} \\ \text{altitudes}}} (\epsilon_j \dot{h}_j - S_j)^2 \quad , \tag{3}$$

*The present mesh triangulation has been chosen for simplicity. Many other grid meshing schemes are, of course, possible; and many of the alternative schemes should be investigated in future work. It is interesting to note, however, that numerous MFE results confirm that PDE solution approximants of higher degree are not nearly so critical for attaining high levels of stability, accuracy, and resolution in an optimal moving node solution method as they are in fixed node or less optimal adaptive PDE solution methods.

calculations, and cylindrical co-ordinates are to be used for HOB calculations. Numerous node control strategies have been tested with alternative penalty function formulations in the regularization terms of Equations(4). The treatment of boundary nodes is particularly significant and suggests that alternative grid mesh triangularizations are needed for the most effective solution of irregular shock reflection problems. Finally, alternative matrix solvers have been tested and implemented in the stiff ODE solver of the MFE airblast code. Widely varying convergence properties and computational efficiencies were observed for various candidate matrix solution methods, and it appears that either ADI methods or our recently developed iterative multigrid type solver will be most desirable for irregular shock reflection problems.

2.2 DISCUSSION OF RESULTS.

The most significant results which emerged from the above tasks are highlighted here. (A detailed description of every important code implementation and every important code test performed in this work would be too voluminous to be very useful.)

2.3 MOTIVATION FOR MFE SOLUTIONS OF NAVIER-STOKES EQUATIONS FOR SHOCKS.

It is useful to first consider the development of the Navier-Stokes equations in 1-D in the context of kinetic theory. Recall that the fluid equations can be written as:

$$\frac{\partial}{\partial t} + \frac{\partial}{\partial x}(\rho v) = 0 \tag{5}$$

$$\frac{\partial(\rho v)}{\partial t} + \frac{\partial}{\partial x}(\rho v^2) = -\frac{\partial}{\partial x}\left\{ p^{(0)} + p^{(1)} + p^{(2)} + \ldots \right\} \tag{6}$$

$$\frac{\partial E}{\partial t} + \frac{\partial}{\partial x}(Ev) = -\frac{\partial}{\partial x}(pv) - \frac{\partial}{\partial x}\left\{ q^{(0)} + q^{(1)} + q^{(2)} + \ldots \right\} \quad . \tag{7}$$

A zero-th approximation of the kinetic theory for gases uses the constitutive relations for an inviscid, non-conducting fluid; i.e.,

$$p = p^{(0)} = \frac{\rho RT}{A} = (\gamma - 1)(E - \frac{1}{2}\rho v^2) \tag{8}$$

$$q = q^{(0)} = 0 \tag{9}$$

These relationships yield the well-known, inviscid Euler equations.

A first approximation of the kinetic theory for gases gives the Navier-Stokes equations according to:

$$p = p^{(0)} + p^{(1)} = (\gamma - 1)(E - \frac{1}{2}\rho v^2) + \frac{4}{3}\mu\frac{\partial v}{\partial x} \tag{10}$$

$$q = q^{(0)} + q^{(1)} = -\kappa\frac{\partial T}{\partial x} \quad . \tag{11}$$

A second approximation of kinetic theory gives the Burnett equations, etc.

The issue of primary concern centers around the potential significance of the physical dissipation processes as determinates of macroscopic flow properties in transient shock interaction regimes. From the standpoint of physics computations, we must distinguish the relative roles in code calculations of numerical dissipation vis à vis the physical dissipation effects which appear on the right hand sides of Equations (6) and (7). A simple shock-boundary layer reflection process has recently been solved by the MFE method in 1-D, which addresses this central issue directly; it is the so-called anomalous wall heating problem. In this problem, anomalously high temperatures are calculated by existing shock hydrodynamics codes for the reflection of a planar shock in an ideal gas from an infinitely reflecting wall in slab geometry (or for an imploding shock reflecting from the origin in spherical or cylindrical co-ordinates). The MFE results which follow indicate that the anomalous aspects are eliminated when numerical dissipation is suppressed and, most important, when the physical dissipation processes in the Navier-Stokes equations are accurately resolved in the transient reflection process. The following test problem in 1-D slab geometry illustrates these results:

Initial Conditions:

$\rho(x, 0) = 1$	$0. \leq x \leq 2.$
$p(x, 0) = \varepsilon(x, 0) = 0$	$0. \leq x \leq 2.0$
$v(x, 0) = -1$	$\Delta x_0 \leq x \leq 2.0$
$v(x, 0) =$ linear	$0 \leq x \leq \Delta x_0$
$v(x, 0) = 0$	$x = 0.$
$\gamma = 5/3$	

Boundary Conditions:

Reflection at $x = 0.$
Dirichlet at initial values at $x = 2.0$

Rankine-Hugoniot Solutions for Infinite Shock ($t \to \infty$):

$s = 1/3$

$\rho^+ = 4.0$;	$\rho^- = 1.0$
$\varepsilon^+ = 0.5$;	$\varepsilon^- = 0.$
$v^+ = 0.$;	$v^- = -1.$
$p^+ = 1.33$;	$p^- = 0.$

The time evolution of this shock was solved by the MFE method in two ways: First the full Navier-Stokes equations were solved accurately using alternative values of $\nu = 4\mu/3$ and κ. These solutions are denoted by N-S in the accompanying figures. In one set of N-S solutions, $\nu = \kappa = 0.01$, which is unrealistically large but which permits comparisons to other fixed node PDE solutions that may use on the order of 100 to several hundred grid nodes. In another set of N-S solutions, $\nu = \kappa = 0.001$, which approximates physically realistic values for actual dissipation processes in gases. Second, the variable ε denotes internal energy per unit mass in the accompanying figures, and anomalous diffusion (denoted by A in the accompanying figures) was simulated by including a diffusion term $\nu_r \rho_{xx}$ in Equation (1). This effectively simulates some form of uncontrolled numerical diffusion which is present intrinsically in all numerical PDE solution methods, and is the only source of dissipation in solutions of the inviscid Euler equations. In the results which follow, we have verified that the MFE solutions of the Navier-Stokes equations have reduced all numerical or other diffusion effects to imperceptible low levels and that the observed behavior of shock interactions is associated with physical dissipation processes.

At $t = 0_+$, the shock incident on the origin is in the incipient state of outward reflection. At $t = 0.05$, Figures 4 and 5 show that the calculations

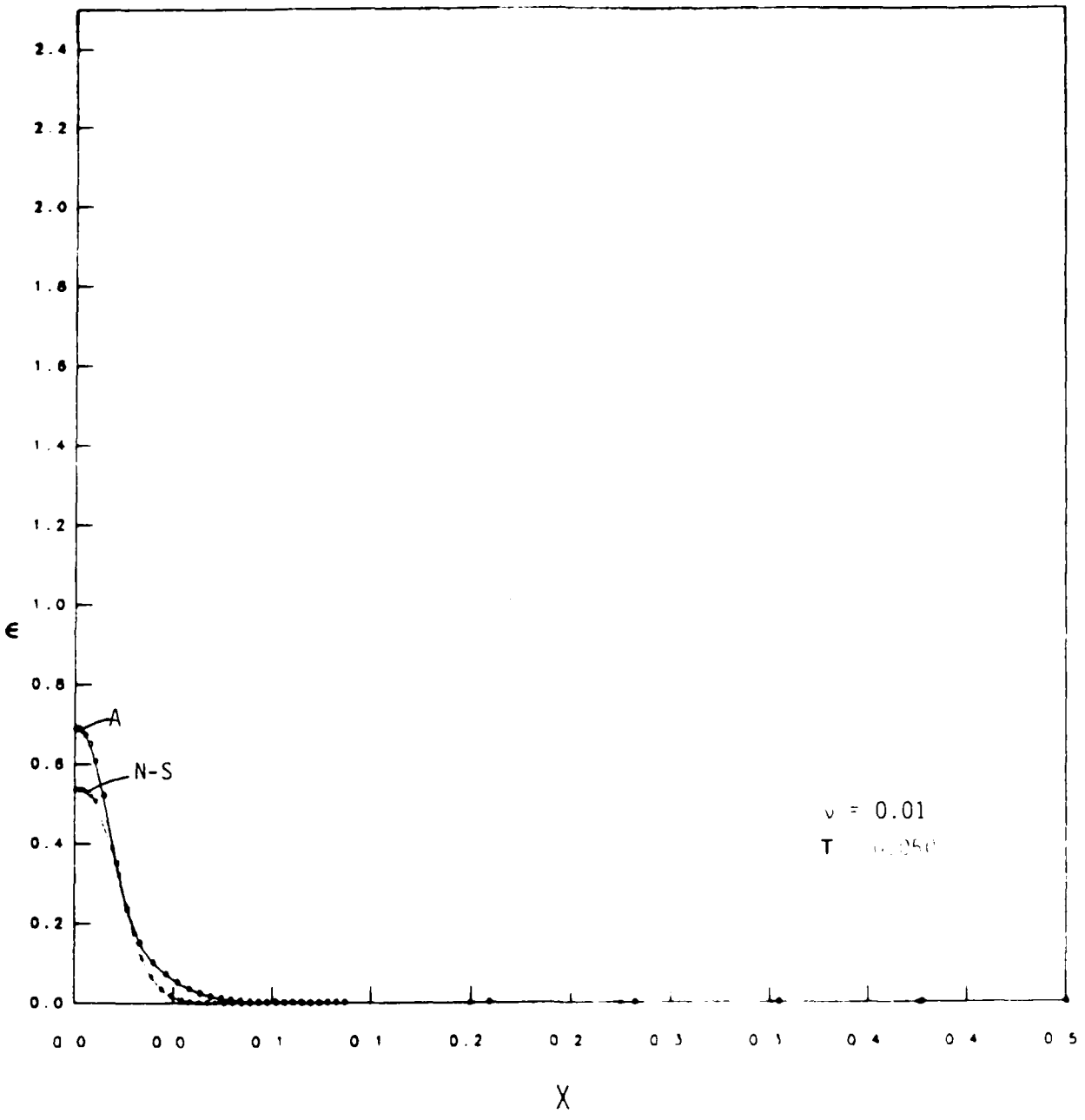

Figure 4. MFE solutions of the Navier-Stokes equations and anomolously dissipative equations at time = 0.050.

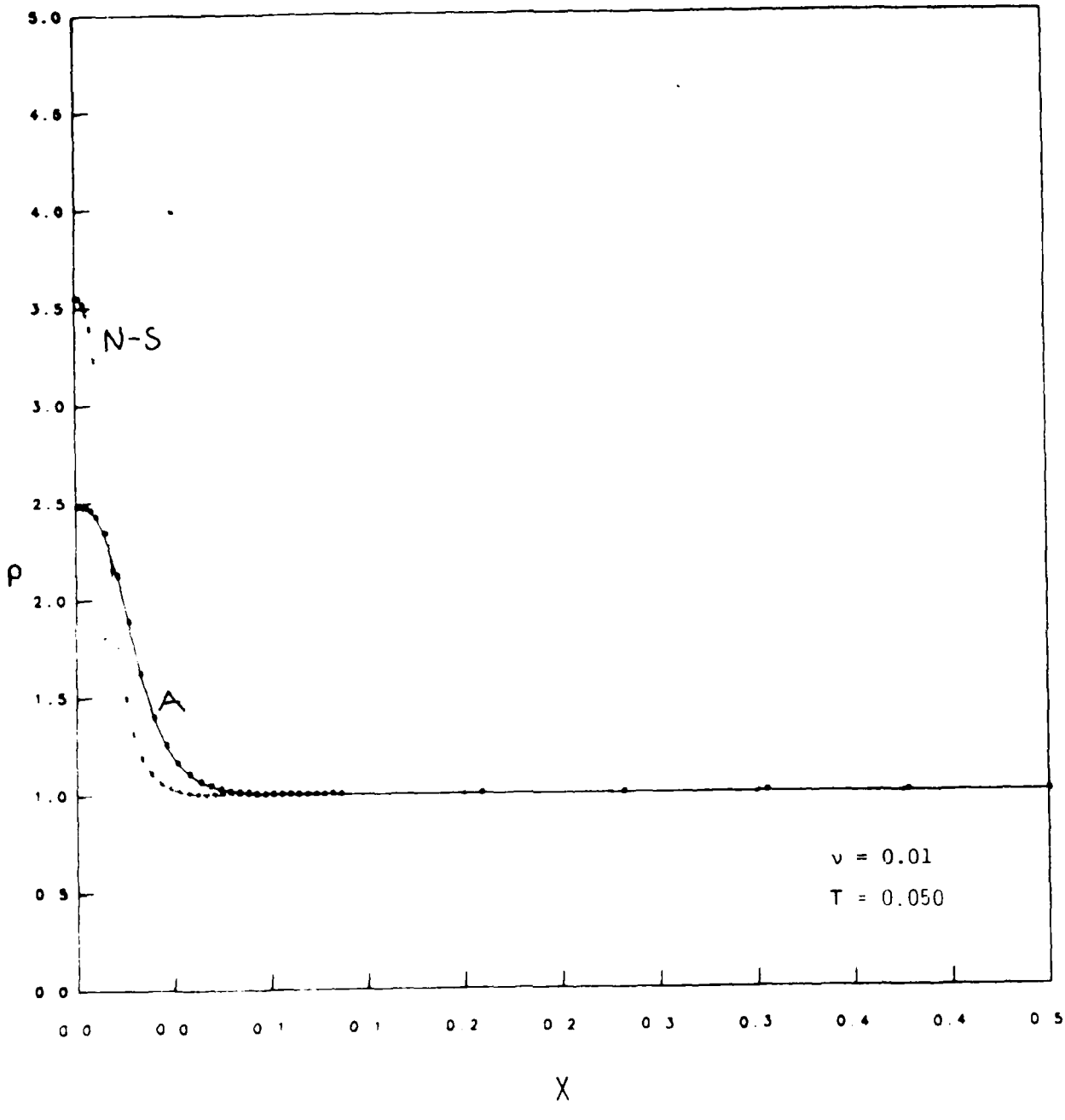

Figure 5. MFE solutions of the Navier-Stokes equations and anomously dissipative equations at time = 0.050.

of the reflected shock with uncontrolled diffusion (or simulated numerical diffusion) tend immediately to overheat in ε and to correspondingly undershoot in ρ relative to the Navier-Stokes solutions. Although these transient solutions are not near their steady state values at this early time, it will be seen that the ensuing evolution toward equilibrium is quite sensitive to both the magnitudes and the nature of the dissipation processes in the computations.

Figure 6 shows that, at $t = 0.15$, the lip of the shock in the Navier-Stokes solution is approaching the steady state value of $\rho = 4.0$, and the anomolous dissipation solution lags by a significant margin. The fluid build-up at the front of the shock is evident here because the fluid near the origin has stagnated while additional fluid continues to stream in toward the origin from the region to the right of the shock. Figure 7 shows that the anomolous dissipation results continue to lag behind the Navier-Stokes solutions to a significant degree at $t = 0.300$. At $t = 2.0$, the Navier-Stokes solutions have approached steady state Rankine-Hugoniot conditions (not shown in Figure 8), and the anomalous dissipation solution has still not reached the Rankine-Hugoniot values in the vicinity of the origin. The anomalous wall heating effects due to uncontrolled dissipation in the density equation have thus persisted to very long times vis à vis the accurate solutions of the Navier-Stokes equations. Non-physical dissipation which is sometimes introduced as artificial viscosity terms in fluid calculations can be shown to have similar anomalous effects, as can the numerical dissipation and/or numerical uncertainties which are present in solvers of inviscid Euler equations.

Figures 9 and 10 present the results of another test of sensitivity of the Navier-Stokes solutions to non-optimal grid locations. In this test problem, a physically realistic value of $\nu = 0.0001$ is used in MFE solutions of the Navier-Stokes equations. We have, however, deliberately constrained the MFE grid nodes in this test case so that they do <u>not</u> migrate to their truly optimal locations, as in the results considered previously. Figure 9 shows several significant features: (i) the shock gradients associated with $\nu = 0.0001$ are extremely large; the accurate resolution of these gradients would require several thousand nodes if a fixed node PDE solution method were to be used, (ii) the Rankine-Hugoniot solutions are approached much more rapidly

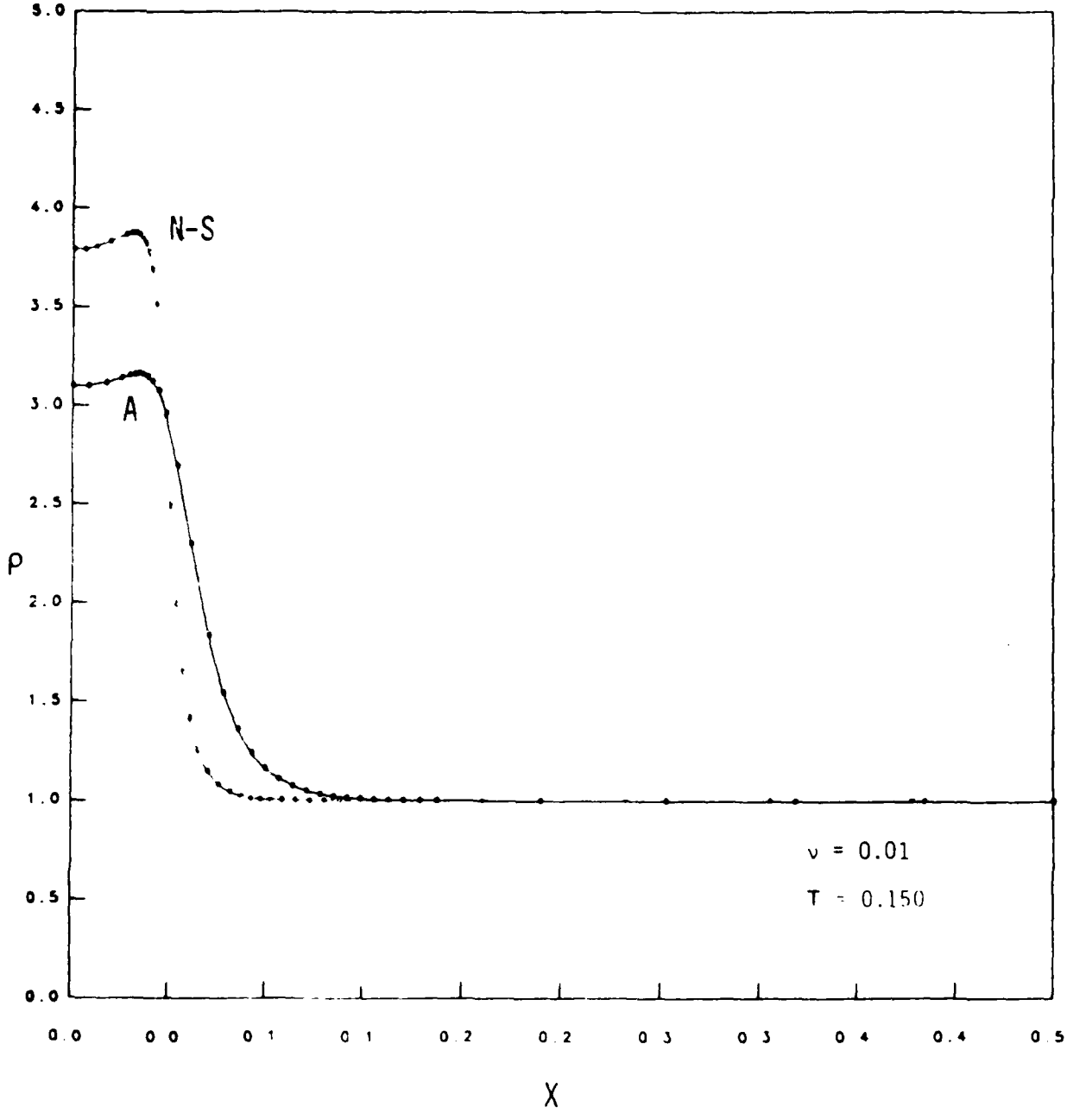

Figure 6. MFE solutions of the Navier-Stokes equations and anomously dissipative equations at time = 0.150.

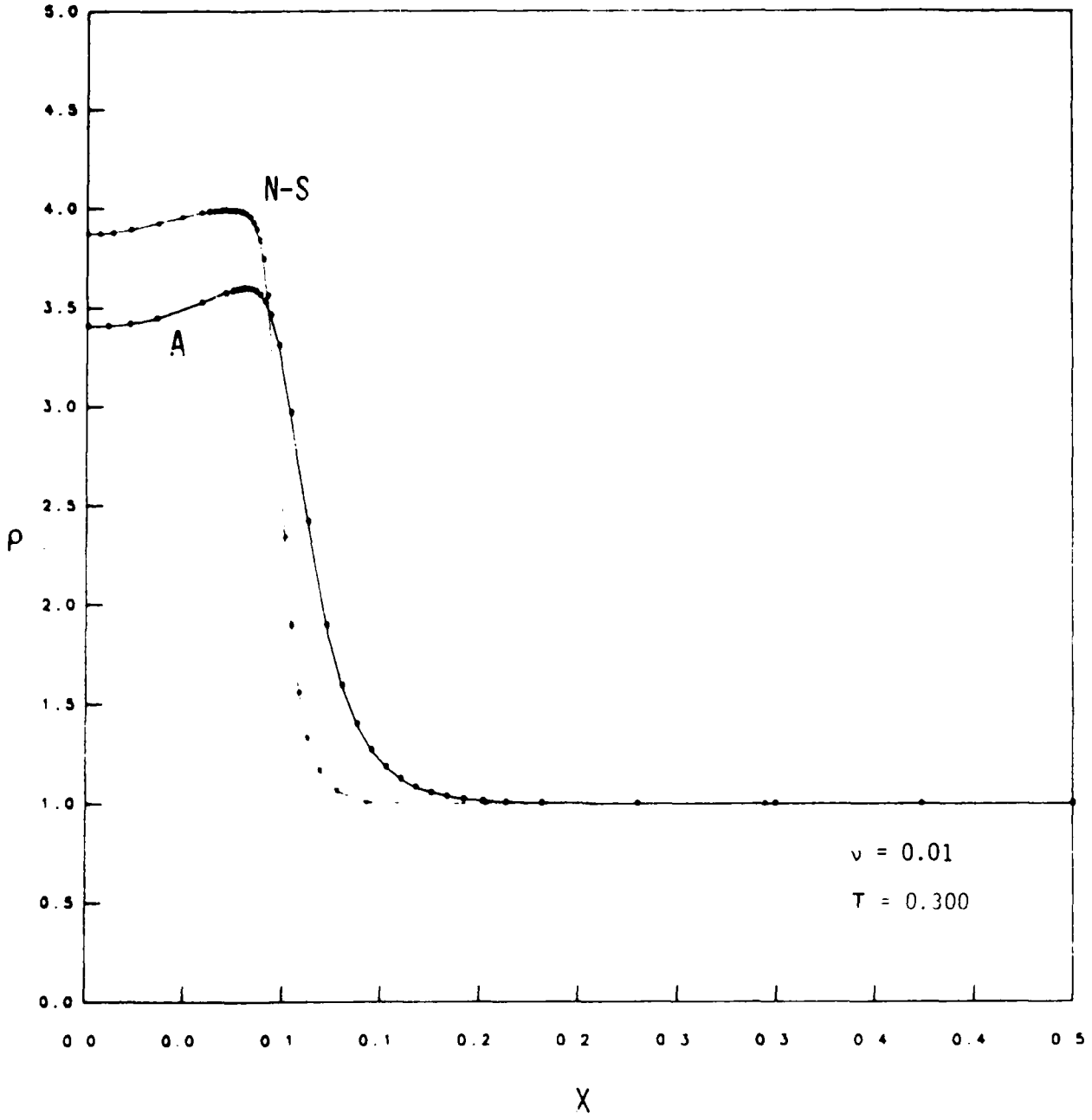

Figure 7. MFE solutions of the Navier-Stokes equations and anomously dissipative equations at time = 0.300.

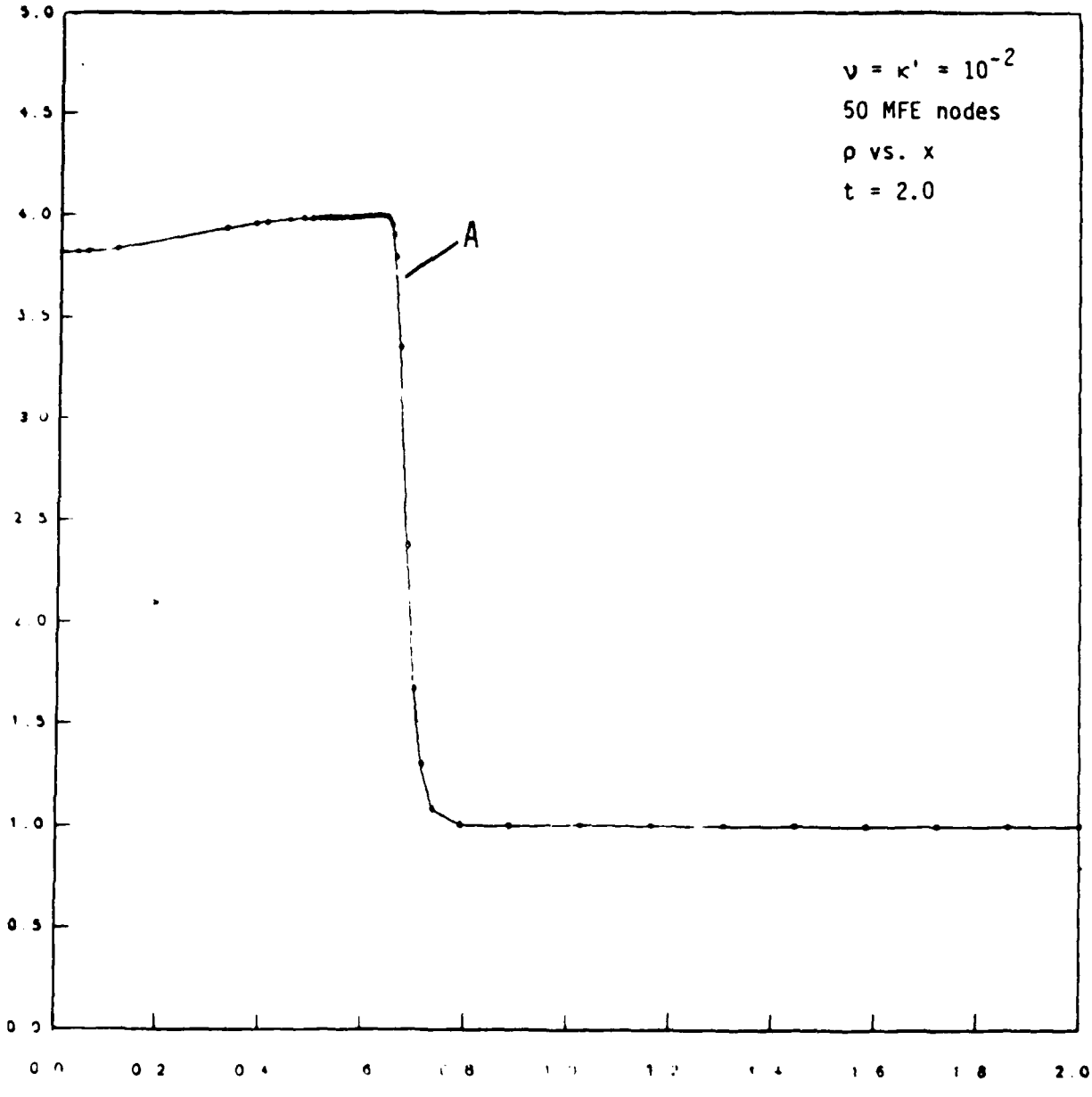

Figure 8. MFE solutions of the Navier-Stokes Equations and anomously dissipative equations at time = 2.0.

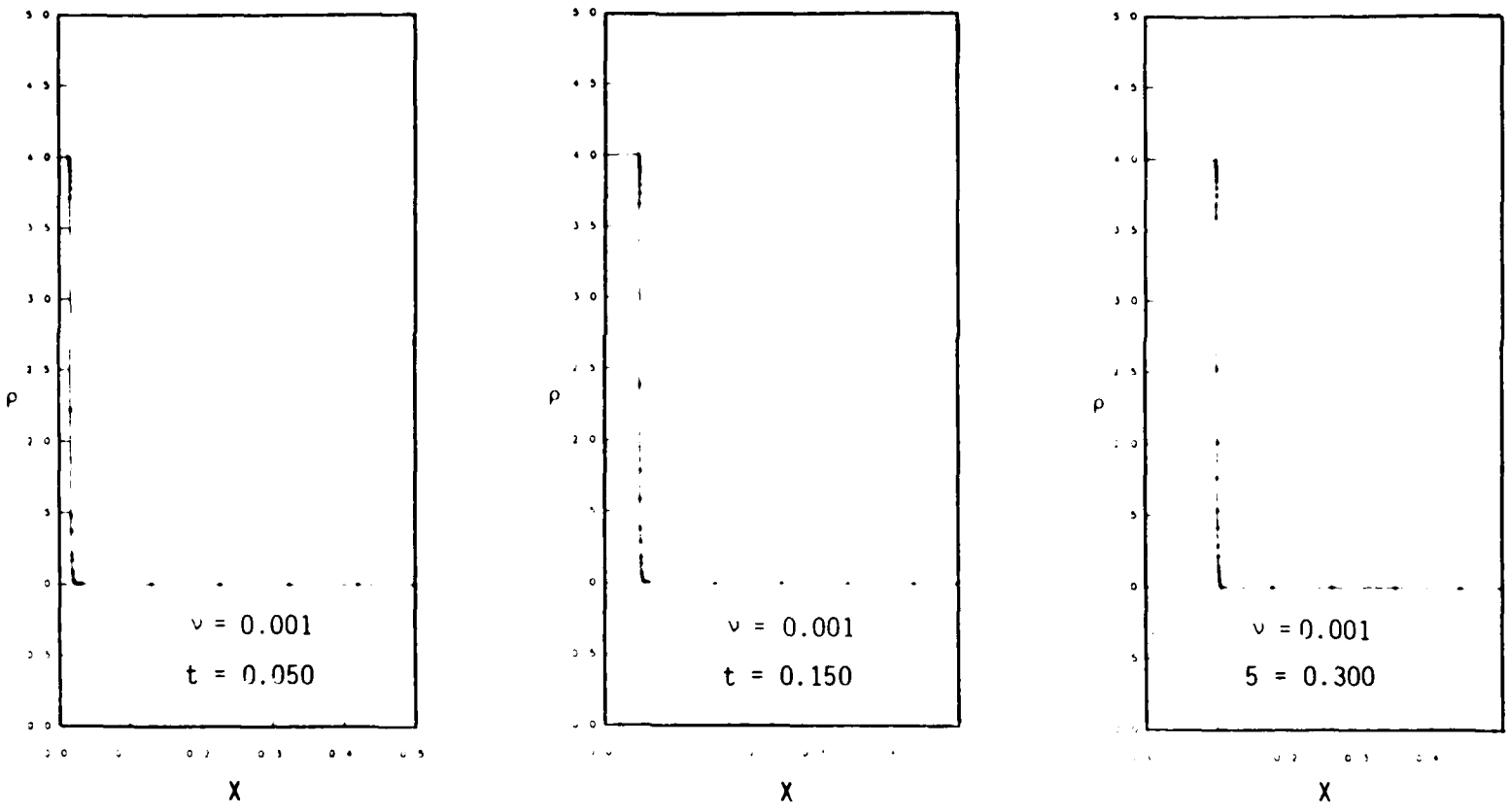

Figure 9. MFE solutions of Navier-Stokes equations with some deliberately constrained grid nodes.

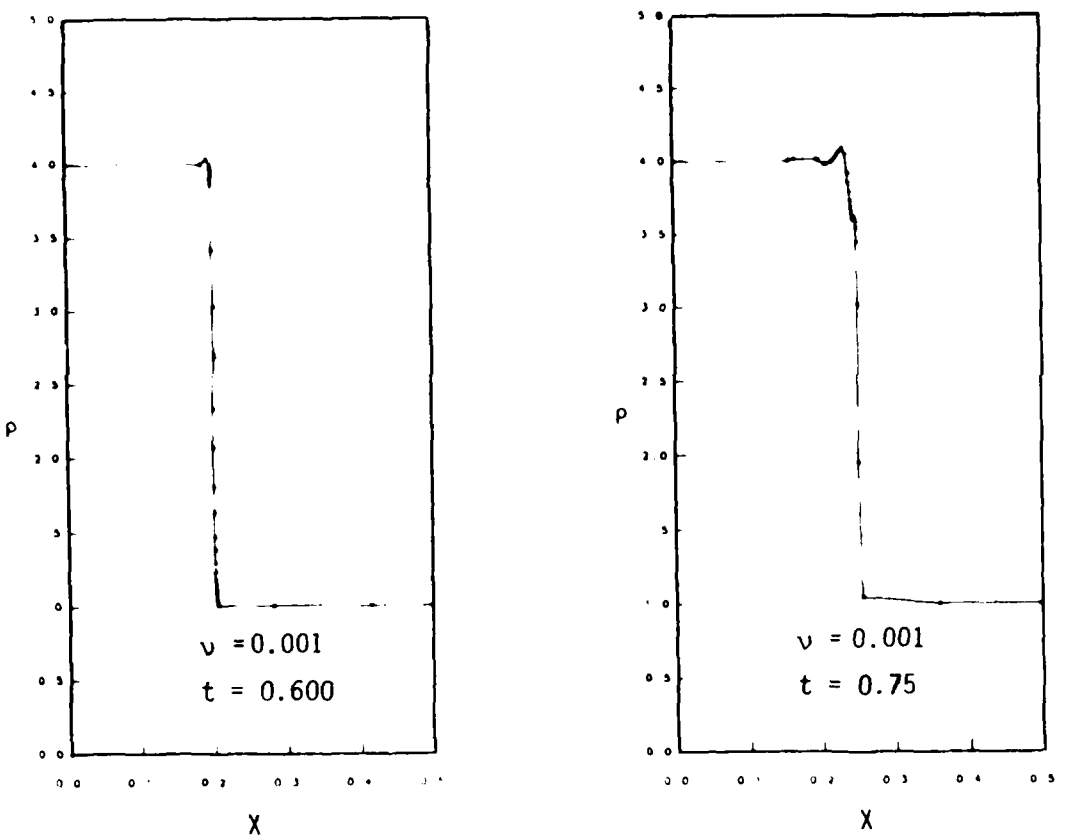

Figure 10. MFE solutions of the Navier-Stokes equations with some deliberately constrained grid nodes.

for the physically realistic values of ν than for the larger values of ν which are typically used either tacitly or explicitly in many other PDE solution methods, and (iii) the slight constraint on node movements and thus on nodal positions do not show up immediately; but once the perturbation becomes significant (as seen in Figure 10), its effects can grow rapidly. In summary, these results demonstrate that reflected shock solutions can be very sensitive to non-physical dissipation effects and to slight deviations from optimal grid node positioning, even in adaptive gridding methods. All of the results in this section were obtained with approximately 30 MFE nodes. As many as 61 MFE nodes were used to verify that the MFE solutions were in fact converged solutions. We have also compared the steady state MFE solutions of fluid velocities with the analytic Navier-Stokes solutions of the steady shock. Excellent agreement was obtained between the MFE solution and the analytic Navier-Stoke solution. In contrast, it was found after extensive attempts that computed solutions which contained nominal degrees of numerical or other anomolous diffusion could not be forced by parameter manipulations to agree with the analytical shock solutions. In still other MFE calculations, we have computed in 1-D the interaction of a shock with an internal shear layer associated with a contact discontinuity -- in direct analogy to the irregular shock reflection mechanisms which occur in higher dimensions. Here also, the computed macroscopic flow properties were sensitive to accurate resolution of the physical dissipation processes in the full Navier-Stokes equations. In the absence of the stringent tests of convergence which were applied here, it can be extremely difficult to discern physical oscillations and dissipation effects from non-physical and/or purely numerical oscillations and dissipation effects. We have, in fact, found it generally impossible to simulate the effects of the actual physical dissipation processes in shock-boundary layer interactions by the use of either artificial or parametrically controlled numerical diffusion processes in Euler equation solutions.

2.4 MFE DEVELOPMENTS IN 2-D.

The 2-D MFE airblast code is being benchmarked extensively against what we consider standard test problems. A first benchmark is the wall heating problem discussed above, and a second set of benchmarks is the shock-on-wedge data of Glass and co-workers for the various types of regular and irregular reflections of plane shocks in Ar. All of these problems are addressed in

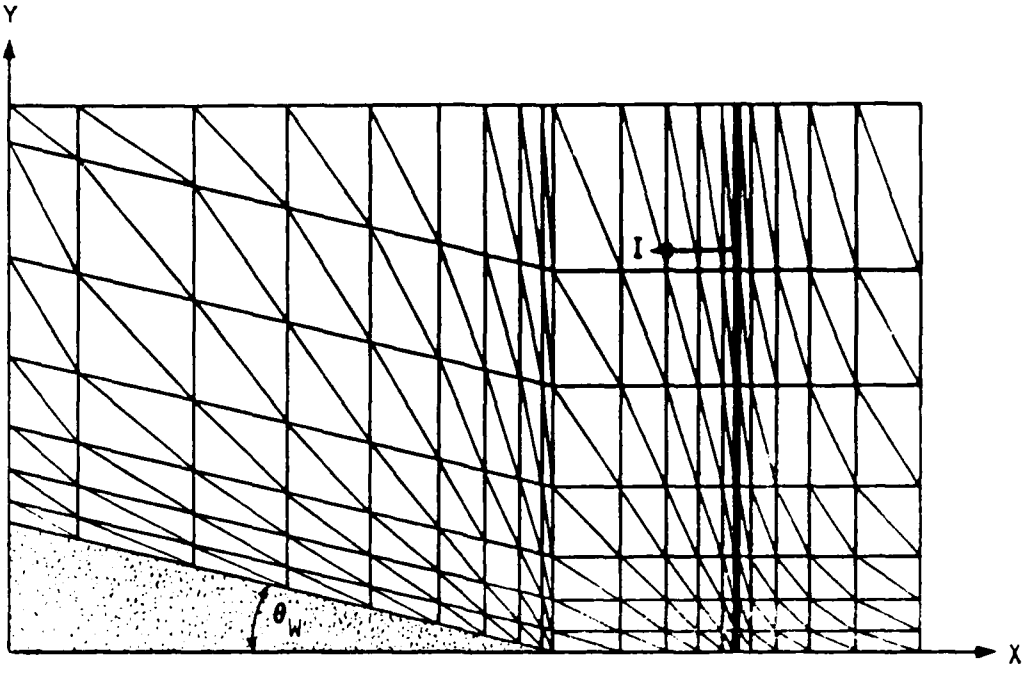

Figure 11. MFE initial grid zone configurations.

rectangular coordinates, as shown by the schematic view of an initial grid mesh configuration in Figure 11.

It was found in this work that the mass, momentum, total energy representation (ρ, $\underline{m}$, E) of the fluid equations has better numerical properties for MFE code calculations than the velocity representation. The Navier-Stokes equations in the (ρ, $\underline{m}$, E) representation are given by

$$\frac{\partial}{\partial t} + \underline{\nabla} \cdot \underline{m} = 0 \tag{12}$$

$$\frac{\partial \underline{m}}{\partial t} + \underline{\nabla} \cdot (\underline{m}\,\underline{m}/\rho) = \underline{\nabla} \cdot \underline{\underline{\Sigma}} \tag{13}$$

$$\frac{\partial E}{\partial t} + \nabla \cdot (E\underline{m}/\rho) = -\underline{\nabla} \cdot \underline{Q} + \nabla \cdot (\underline{\underline{\Sigma}} \cdot (\underline{m}/\rho)) \quad , \tag{14}$$

where $\underline{\underline{\Sigma}}$ is the generalized stress tensor and $\underline{Q}$ is the heat flux vector. The heat flux vector is frequently given by

$$\underline{Q} = - \kappa \underline{\nabla} T \quad , \tag{15}$$

where T is the temperature. The general stress tensor is frequently given by

$$\underline{\underline{\Sigma}} = -p\underline{\underline{I}} + \underline{\underline{\tau}} \quad , \tag{16}$$

where $\underline{\underline{I}}$ is the identity matrix. For an ideal gas (a Newtonian fluid) in Cartesian co-ordinates

$$p = p^{(0)} = (\gamma - 1)(E - m^2/2\rho), \text{ and} \tag{17}$$

$$\tau_{xx} = 2\mu \frac{\partial(\underline{m}/\rho)_x}{\partial x} - \frac{2}{3}\mu(\underline{\nabla} \cdot (\underline{m}/\rho)) \tag{18}$$

$$\tau_{yy} = 2\mu \frac{\partial(\underline{m}/\rho)_y}{\partial y} - \frac{2}{3}\mu(\underline{\nabla} \cdot (\underline{m}/\rho)) \tag{19}$$

$$\tau_{xy} = \mu\left[\frac{\partial(\underline{m}/\rho)_x}{\partial y} + \frac{\partial(\underline{m}/\rho)_y}{\partial x}\right] \quad . \tag{20}$$

It is important to note in Equation (13) that the quantity $\underline{m}\ \underline{m}$ is a dyadic. Special attention has been devoted to exacting evaluations of those inner product terms which involve factors of $\frac{1}{\rho}$ for small ρ. These factors are present in all standard representations of the fluid equations. The inner products in the equations above have been coded for calculations in both Cartesian and cylindrical co-ordinates.

The inner product formulation of discretized finite element equations offers a potentially unique advance for the treatment at the origin, as $r \to 0$, of those PDE operators which are proportional to $1/r$. Singularities do <u>not</u> occur because the inner products of the MFE basis functions are weighted by the measures $2\pi r$ in cylindrical co-ordinates. The MFE method is thus intrinsically analytic at the origin in both cylindrical and spherical coordinates which obviates any of the numerical tricks which are otherwise used in discretized PDE solution methods. It has been tested and verified that there is, of course, a price to be paid for the exploitation of this analytic feature. It lies in the fact that node movement properties differ from one to another weighting scheme of MFE norms. Because the MFE method

is still a new PDE solution method in many respects, the specific node movement strategies for cylindrical co-ordinates will have to be tested much further when HOB calculations are undertaken.

2.5 STANDARD TEST PROBLEMS.

As a first standard test problem, the anomolous wall heating problem discussed above was solved as the reflection of a planar shock against a vertical wall in 2-D. It was found using slip boundary conditions that any cut of the 2-D shock profile at constant -y replicated the 1-D results. It was, in fact, found that the 2-D MFE solutions of this problem required fewer time steps for running to completion than the 1-D code required for the corresponding problem to be executed in 1-D. The total computational cost in 2-D nevertheless exceeded the cost for computing this problem in 1-D, because the respective costs per time step are much greater in 2-D than in 1-D. But these results suggest that the additional degrees of topological freedom for MFE node movements in 2-D, vis à vis 1-D, are conducive to intrinsic computational economies in integration time steps.

Physically, this benchmark problem is significant because it contains only fluid compression and expansion effects; fluid shearing and vorticity generation is non-existent. This test problem therefore acts as an effective screening example for both coding and physics validation purposes. It would serve similarly as a useful example for measuring numerical dissipation effects in all existing airblast codes.

The isodensity contour (isopycnic) data from shock tube measurements by Glass and co-workers[1] are perhaps the most highly pertinent data in existence for the fundamental study of those detailed shock-boundary/shear layer interactions which may ultimately govern the transient evolution of irregular shock reflection processes. This data resolves the density profiles in the boundary and internal shear layers. The case of regular shock reflection is shown schematically in Figure 12.

The second standard test considered in this work is the case of regular shock reflection in argon at Mach number $M_s = 2.05$, $p_o = 150$ torr, $\rho_o = 3.23 \times 10^{-4}$ g/cm^3, $T_o = 297.6°K$, and wedge angle $\theta_w = 60°$. This

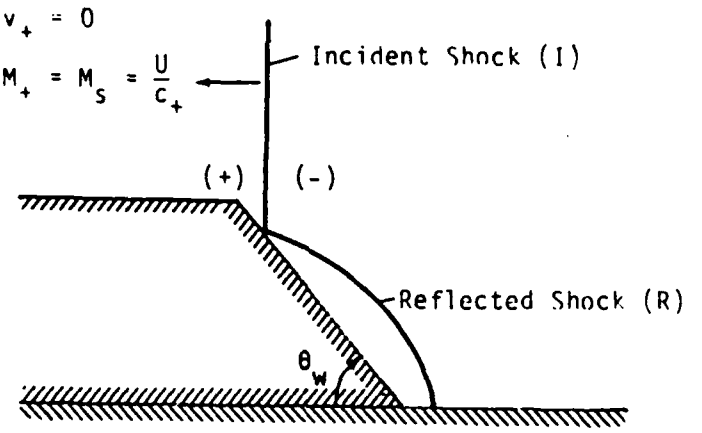

Figure 12. Schematic representation of regular reflection in Shock-on-wedge experiments.

shock has been measured experimentally by Deschambault and Glass.[1] Initial conditions are calculated from the Rankine-Hugoniot relationships in the following form:

$$M_+ = \frac{U - v_+}{C_+} = M_S \quad \text{for } v_+ = 0 \quad , \tag{21}$$

$$C_+ = (\gamma p + /\rho_+)^{\frac{1}{2}} \quad , \tag{22}$$

$$p_- = p_+ \cdot \frac{2\gamma M_+^2 - (\gamma - 1)}{(\gamma + 1)} \quad , \tag{23}$$

where = 5/3 for argon.

$$(u - v_-) = \frac{p_+ - p_-}{\rho_+(u - v_+)} + (u - v_+) \quad , \tag{24a}$$

$$\text{or} \quad v_- = \frac{p_- - p_+}{\rho + u} \quad , \tag{24b}$$

$$\rho_- = \rho_+ \frac{u}{u_- v_-} \quad . \tag{25}$$

For monatomic gases, the internal energy per unit volume is

$$\rho\varepsilon = \frac{3}{2}p \quad . \tag{26}$$

The initial conditions are

$\rho_+ = 3.23 \times 10^{-4}$ g/cm^3
$m_+ = 0$
$E_+ = [\rho_+ \varepsilon_+ + m_+^2/2\rho_+] = 3.0 \times 10^5$ ergs/cm^3 and
$\rho_- = 7.87 \times 10^{-4}$ g/cm^3
$m_- = 30.559$ gm - cm/sec
$E_- = [\rho_- \varepsilon_- + m_-^2/2\rho_-] = 2.132 \times 10^6$ ergs/cm^3

2.6 BOUNDARY CONDITIONS.

A significant point of fundamental physics became manifest in the study of boundary conditions for shock-on-wedge calculations. For a variety of reasons, conventional airblast codes use slip-type boundary conditions. In actuality, the velocity of air molecules is zero at the types of surfaces under present consideration. For the sake of common comparisons, and to test the sensitivity of MFE shock-on-wedge computations to alternative boundary conditions, we first attempted to solve the regular shock-on-wedge test problem with slip-type boundary conditions, in which the normal component of velocity along the bottom horizontal surface and inclined wedge are zero and the tangential velocity components are treated by zero-Neumann (or symmetry) conditions (see Figure 11). These symmetry boundary conditions are applied similarly to the MFE grid nodes so that the grid nodes would slide freely along both the horizontal surface and the inclined wedge surface. But the MFE method has always been found to be extremely sensitive in its accuracy and consistency requirements to the presence of any physical or mathematically ill-posed condition. Here, the surface normal is not defined uniquely

at the front of the wedge. Consequently, the basic consistency requirements in the MFE method impeded the numerical integration process because the symmetry boundary condition at the foot of the wedge is ill-posed, and thus could not be properly resolved as a truly rigorous PDE solution. The MFE method also tends to be less tolerant than most PDE methods of computational swindles which are frequently used to accomplish slip-type boundary conditions. It thus became quite apparent that it is possible to enforce slip-type boundary conditions only by accepting erroneous numerical solutions in the boundary layer region near the front corner of the wedge. It was further apparent that these errors could propagate to regions well away from the local source of difficulty. In view of these results, we next attempted to take a giant step forward in terms of both the physics and computations of the physically required non-slip boundary conditions. This turned out to be a giant step because this shock-on-wedge problem has a turbulent boundary layer in the duct represented by our problem domain. Nevertheless, some key points became manifest in this task which will be described immediately below.

The initial shock conditions are shown in Figure 13. This problem is solved in a 1 cm duct. For viscosity $\mu = 5 \times 10^{-4}$, the Reynolds number is approximately 5.7×10^{4}. Such a flow is clearly turbulent. The MFE solutions of the laminar Navier-Stokes equations were nevertheless attempted as a numerical experiment. These results appear in Figures 14 to 23 with self-explanatory captions. At $t = 0.30$ the shock is just starting to encounter the wedge front; and the isodensity contours early in the reflection process at $t = 0.35$ have a regular profile. At $t = 0.44$ the formation and subsequent shedding of eddies are becoming apparent. These are formed and evolved according to the physically inadequate laminar dissipation processes in the present Navier-Stokes solutions and not by numerical dissipation or by an appropriate turbulence model. Analysis of vorticity generation rates indicates clearly that a turbulent model of the physical dissipation in the boundary layer is required in order to model this system according to physical reality.

Mostly, this example shows an apparent capacity of the MFE method to attempt to resolve extremely micro-scale dissipation processes simultaneously

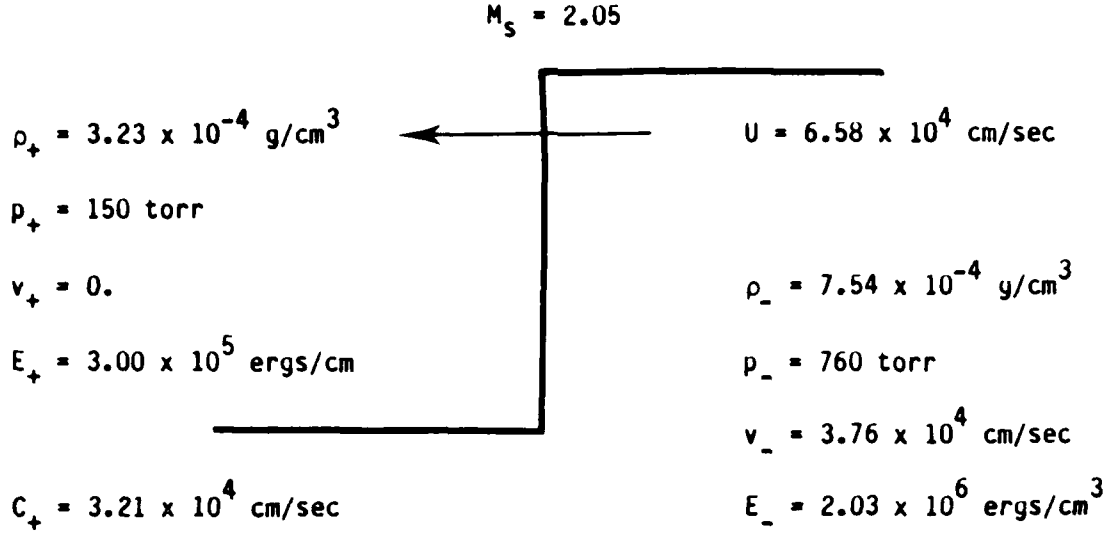

Figure 13. Initial conditions for regular reflection of planar shock in the experiments of Deschambault and Glass.

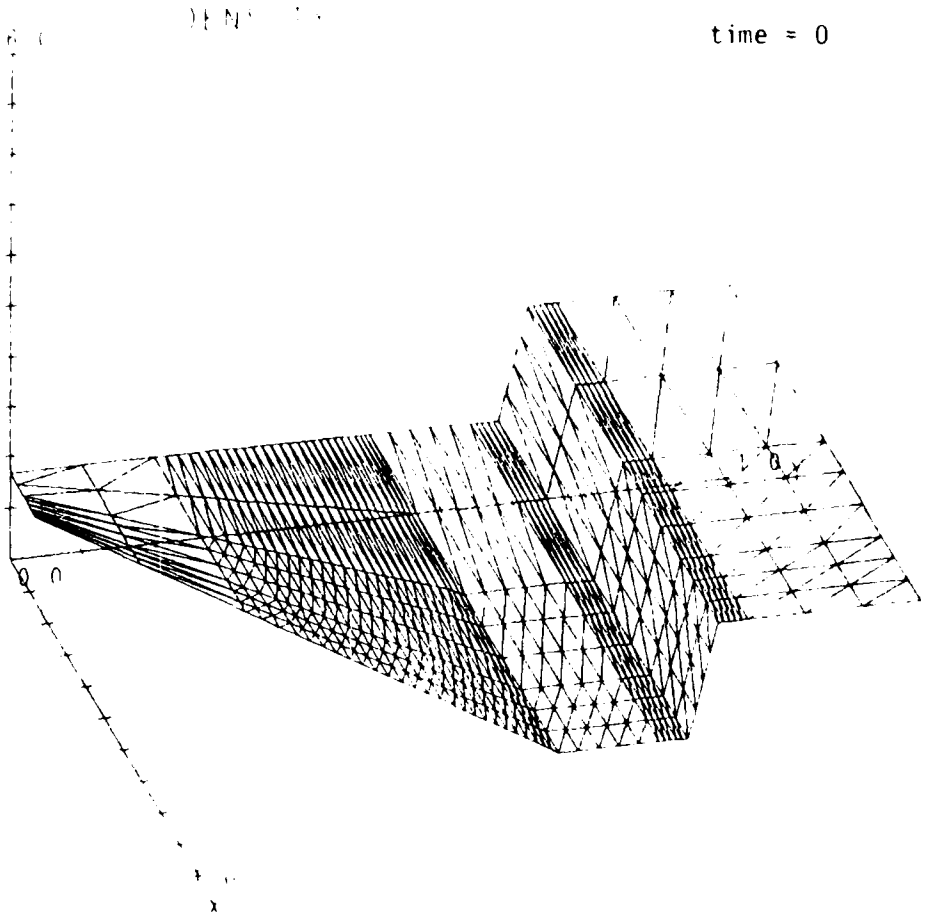

Figure 14. MFE Solutions of Laminar Navier-Stokes Equations for a Regular Shock Reflection Experiment of Deschambault and Glass (M_S = 2.05, Θ = 60°, p_+ = 150 torr, $\rho_+ = 3.23 \times 10^{-4} g/cm^3$ in Argon). The MFE Grid is 9 x 51 Nodes and Non-Slip Boundary Conditions Are Used.

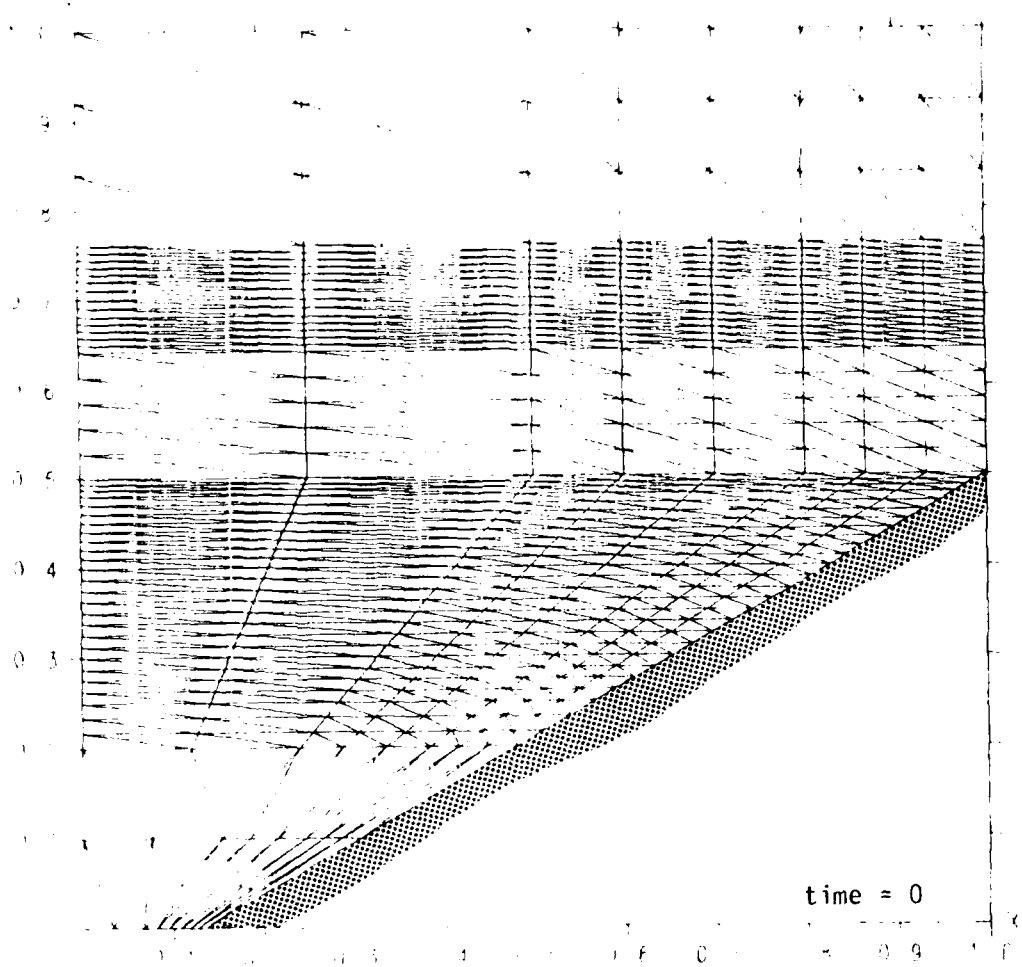

Figure 15. MFE Solutions of Laminar Navier-Stokes Equations for a Regular Shock Reflection Experiment of Deschambault and Glass (M_S = 2.05, Θ = 60°, p_+ = 150 torr, $\rho_+ = 3.23 \times 10^{-4} g/cm^3$ in Argon). The MFE Grid is 9 x 51 Nodes and Non-Slip Boundary Conditions Are Used.

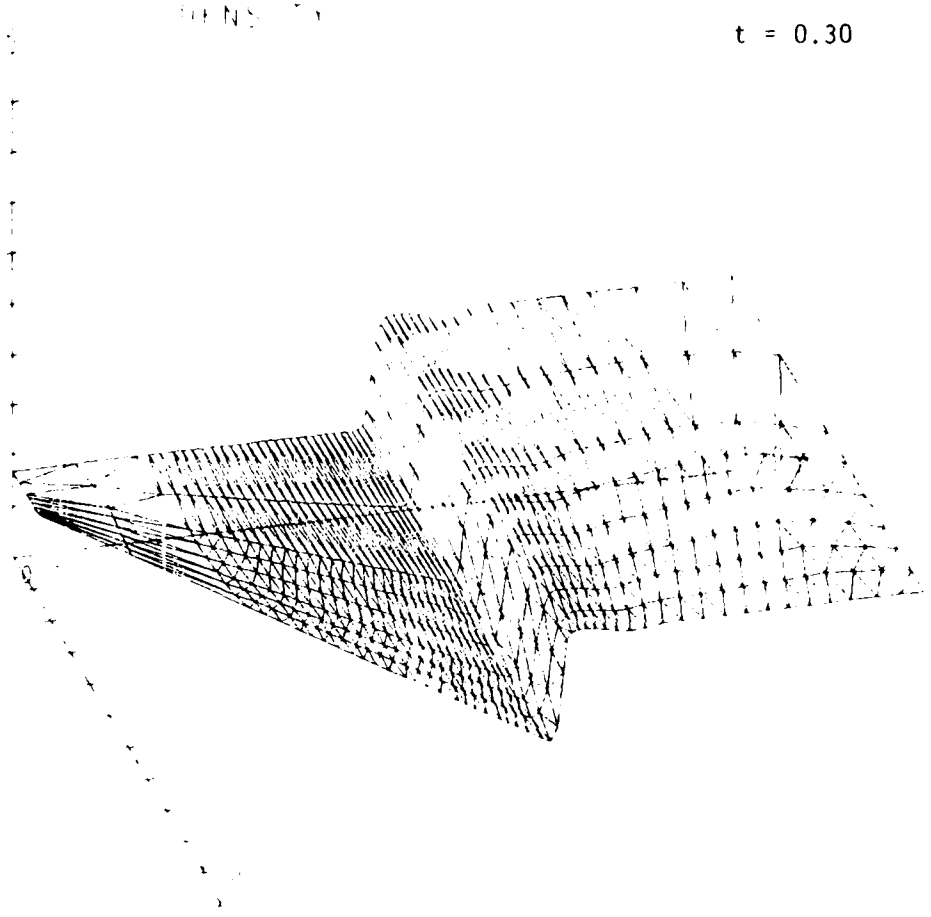

Figure 16. MFE Solutions of Laminar Navier-Stokes Equations for a Regular Shock Reflection Experiment of Deschambault and Glass (M_S = 2.05, Θ = 60°, p_+ = 150 torr, $\rho_+ = 3.23 \times 10^{-4} g/cm^3$ in Argon). The MFE Grid is 9 x 51 Nodes and Non-Slip Boundary Conditions Are Used.

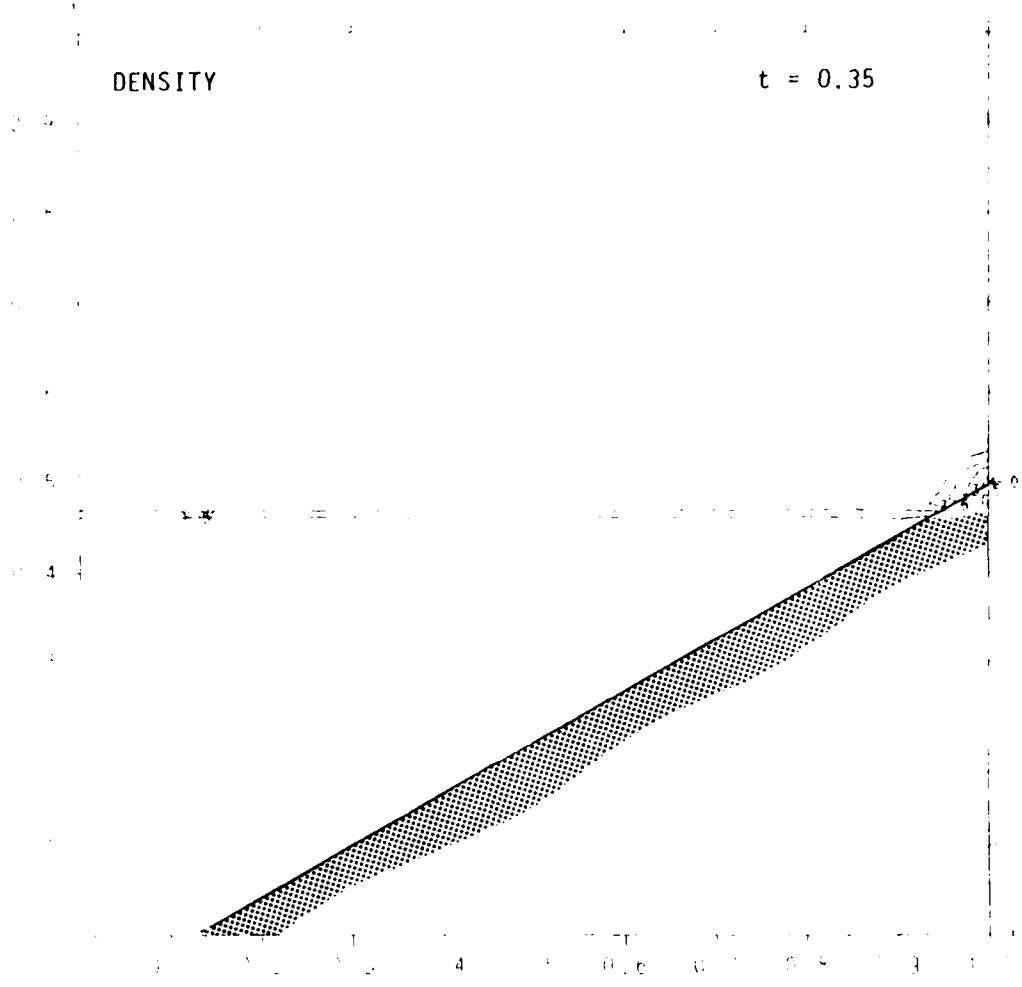

Figure 17. MFE Solutions of Laminar Navier-Stokes Equations for a Regular Shock Reflection Experiment of Deschambault and Glass (M_S = 2.05, Θ = 60°, p_+ = 150 torr, $\rho_+ = 3.23 \times 10^{-4} g/cm^3$ in Argon). The MFE Grid is 9 x 51 Nodes and Non-Slip Boundary Conditions Are Used.

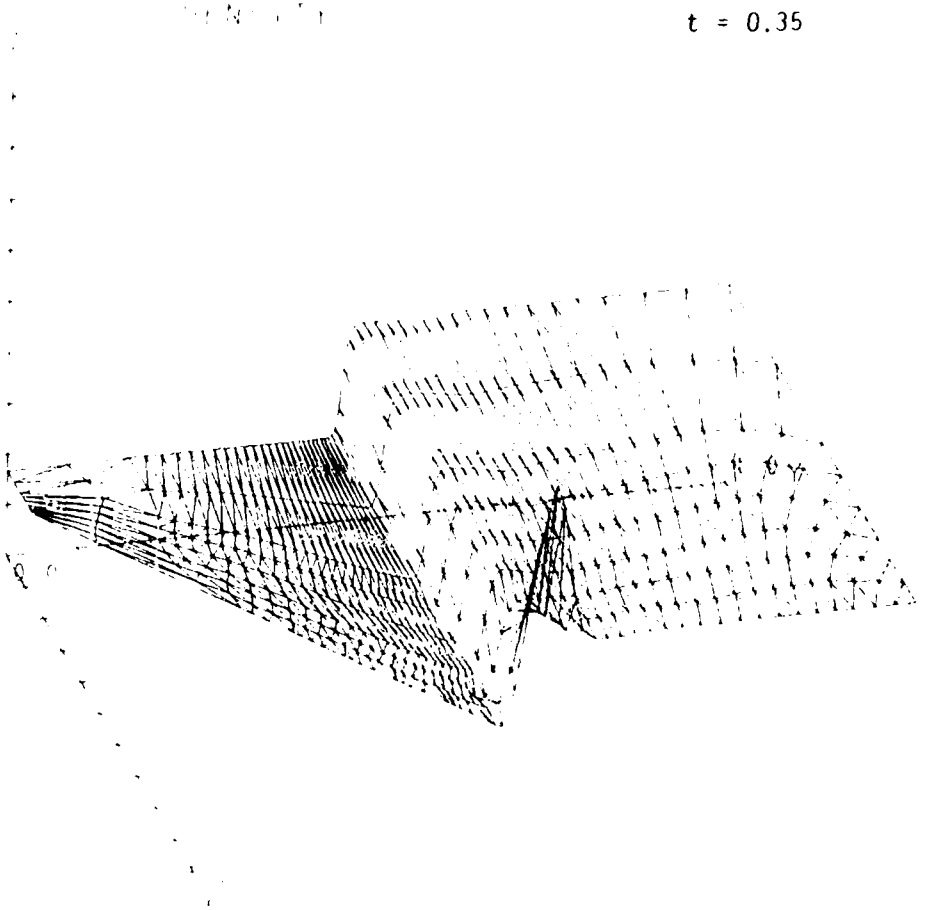

Figure 18. MFE Solutions of Laminar Navier-Stokes Equations for a Regular Shock Reflection Experiment of Deschambault and Glass (M_S = 2.05, Θ = 60°, p_+ = 150 torr, ρ_+ = 3.23 x 10^{-4} g/cm^3 in Argon). The MFE Grid is 9 x 51 Nodes and Non-Slip Boundary Conditions Are Used.

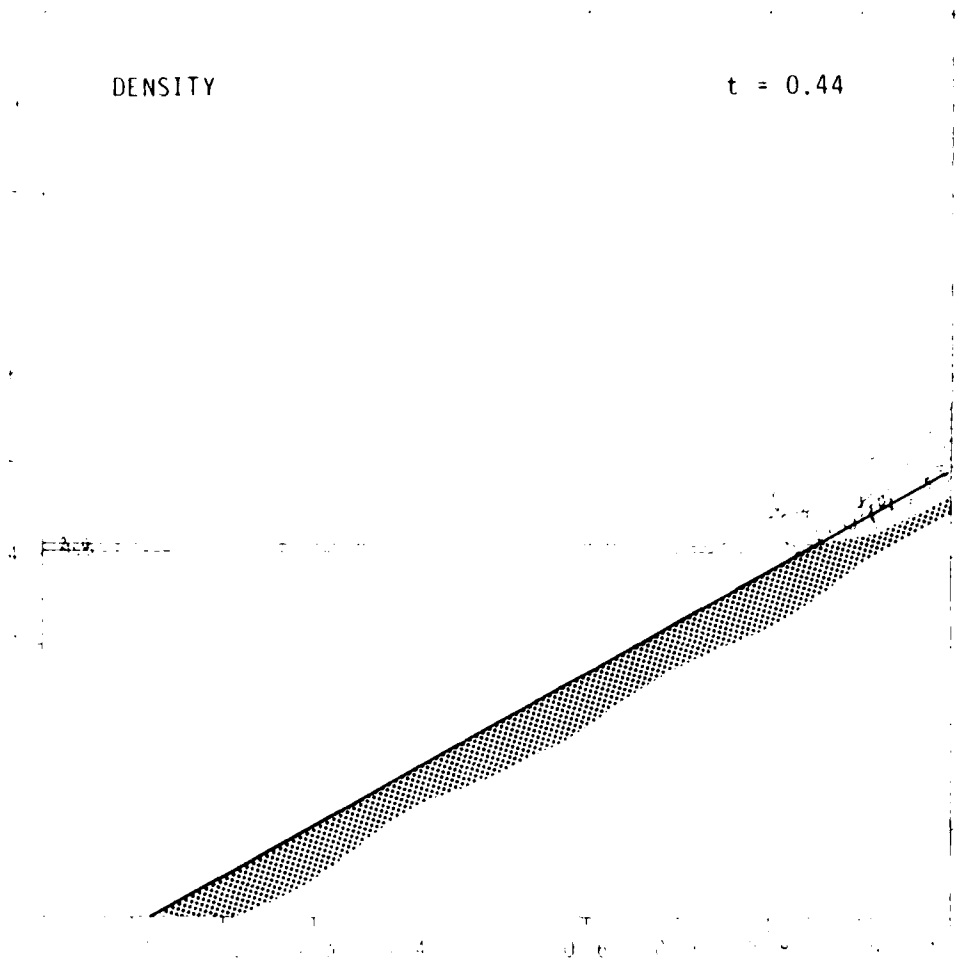

Figure 19. MFE Solutions of Laminar Navier-Stokes Equations for a Regular Shock Reflection Experiment of Deschambault and Glass (M_S = 2.05, Θ = 60°, p_+ = 150 torr, $\rho_+ = 3.23 \times 10^{-4} g/cm^3$ in Argon). The MFE Grid is 9 x 51 Nodes and Non-Slip Boundary Conditions Are Used.

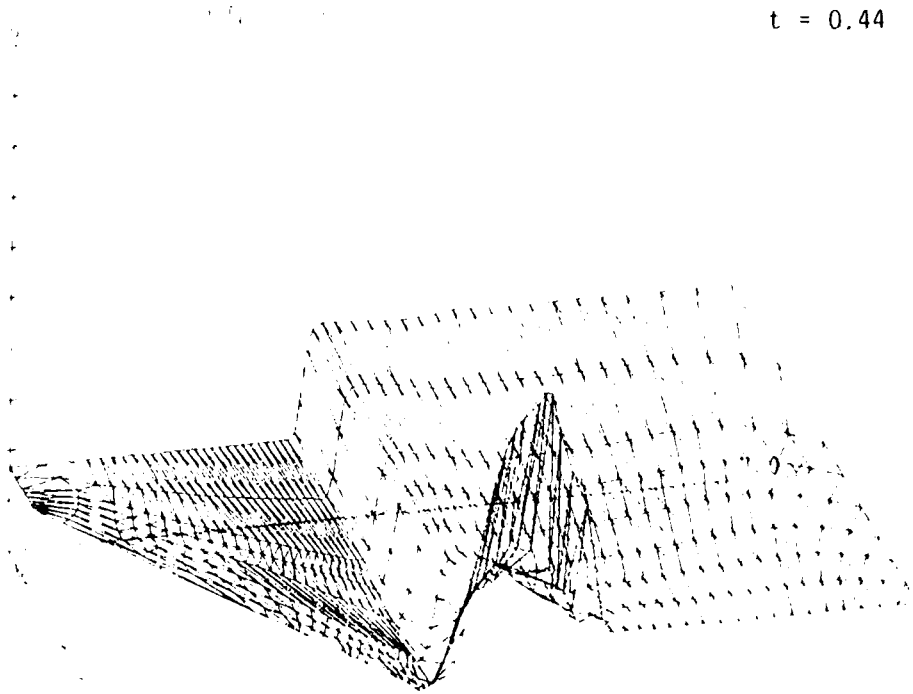

Figure 20. MFE Solutions of Laminar Navier-Stokes Equations for a Regular Shock Reflection Experiment of Deschambault and Glass (M_S = 2.05, Θ = 60°, p_+ = 150 torr, $\rho_+ = 3.23 \times 10^{-4} g/cm^3$ in Argon). The MFE Grid is 9 x 51 Nodes and Non-Slip Boundary Conditions Are Used.

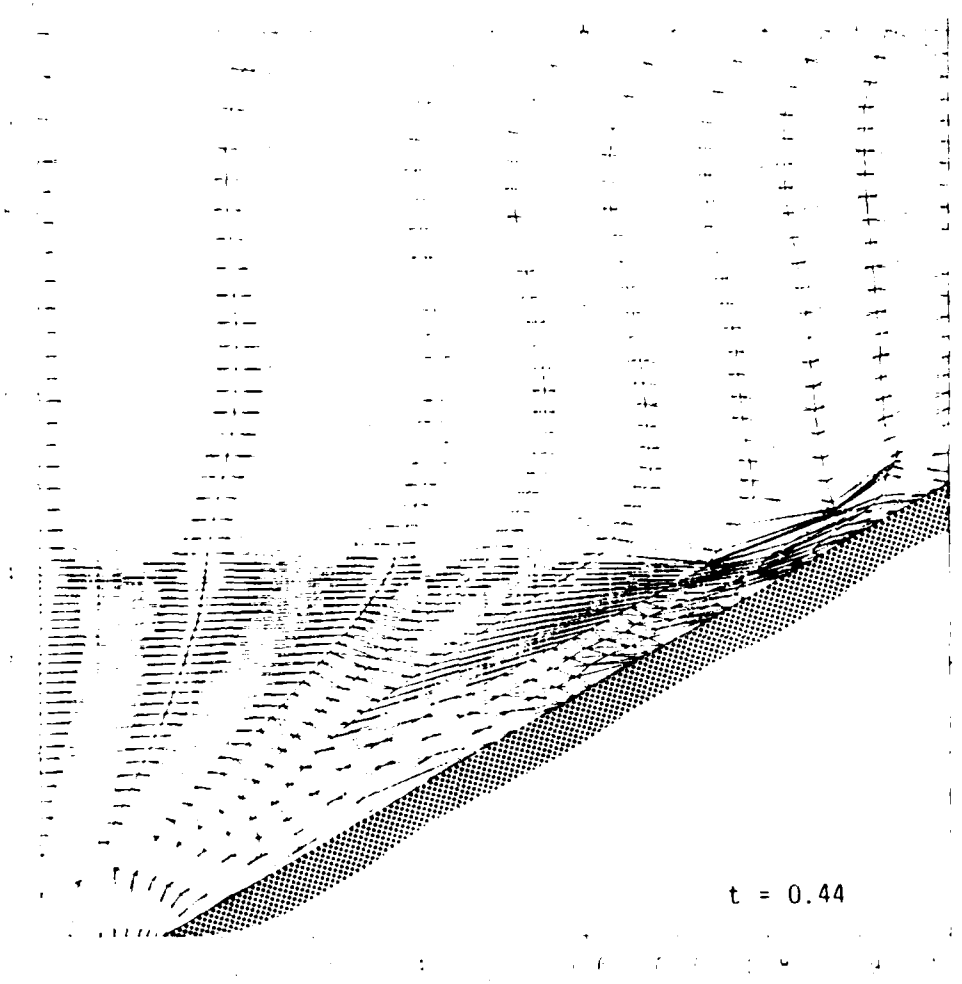

Figure 21. MFE Solutions of Laminar Navier-Stokes Equations for a Regular Shock Reflection Experiment of Deschambault and Glass (M_s = 2.05, θ = 60°, p_+ = 150 torr, $\rho_+ = 3.23 \times 10^{-4} g/cm^3$ in Argon). The MFE Grid is 9 x 51 Nodes and Non-Slip Boundary Conditions Are Used.

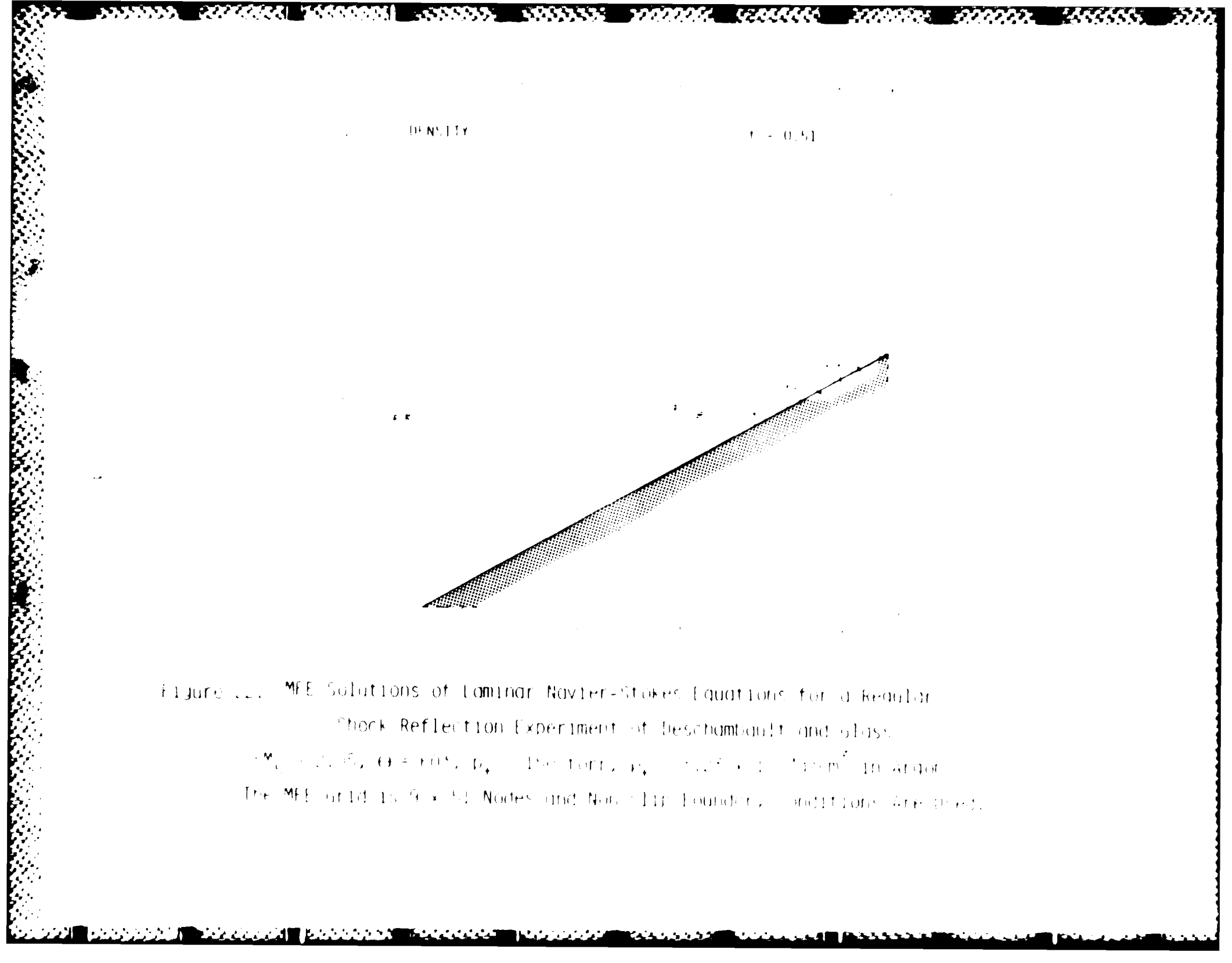

Figure ... MFE Solutions of Laminar Navier-Stokes Equations for a Regular Shock Reflection Experiment of Deschambault and Glass

M_s = ..., θ = ...°, p_∞ = ... torr, p_∞ = ... psi in Argon

The MFE grid is ... x ... Nodes and Non-Slip Boundary Conditions are used.

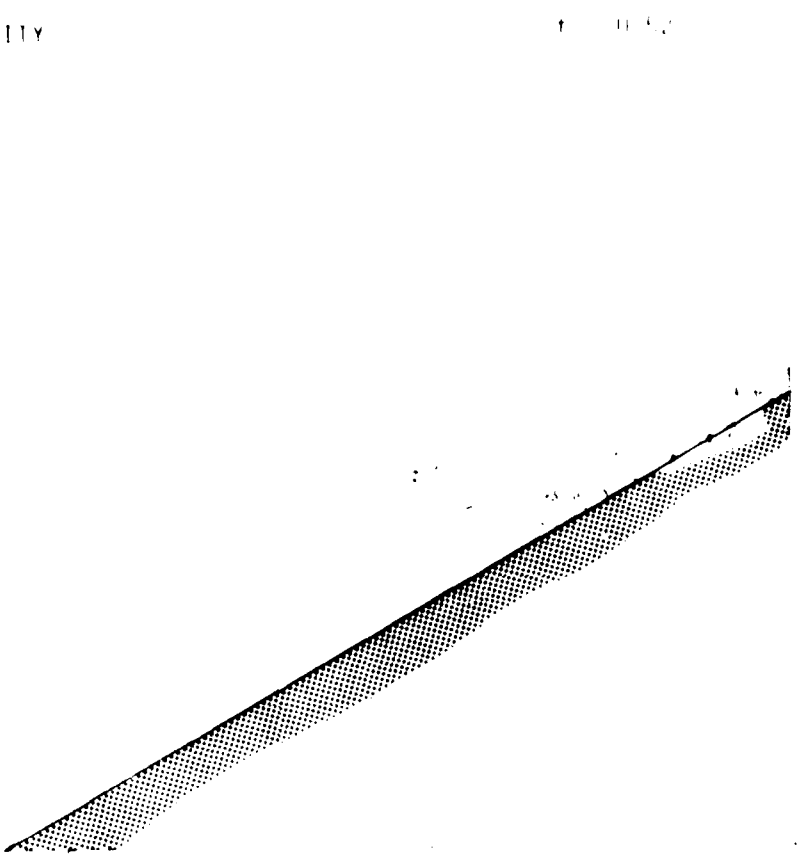

Figure 23. MFE Solutions of Laminar Navier-Stokes Equations for a Regular Shock Reflection Experiment of Deschambault and Glass (M_s = [illegible], θ = 60°, p_+ = 150 torr, $\rho_+ = 3.23 \times 10^{-4}$ g/cm^3 in Argon). The MFE Grid is 9 x 51 Nodes and Non-Slip Boundary Conditions Are Used.

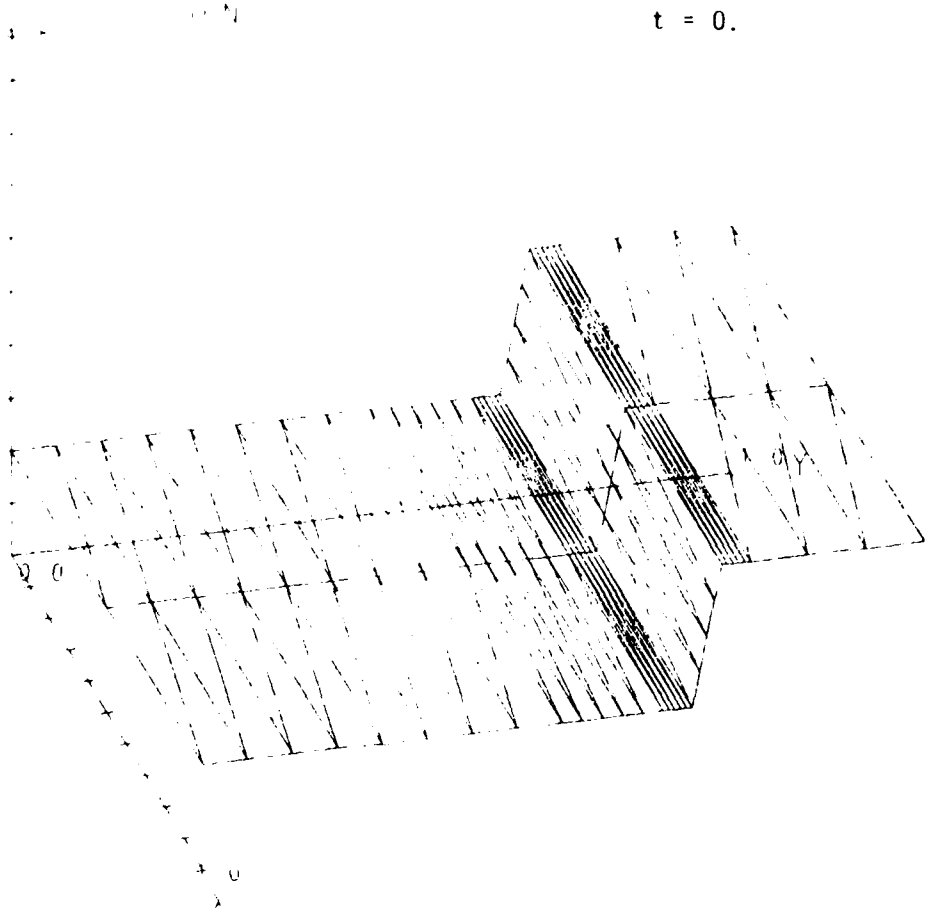

Figure 24. MFE Solutions of Laminar Navier-Stokes Equations for An Experimental Plane Shock of Deschambault and Glass Reflecting Against a Vertical Wall.
(M_S = 2.05, Θ = 90°, p_+ = 150 torr, ρ_+ = 3.23 x 10^{-4}g/cm^3 in Argon).
A 3 x 31 MFE Grid is Used.

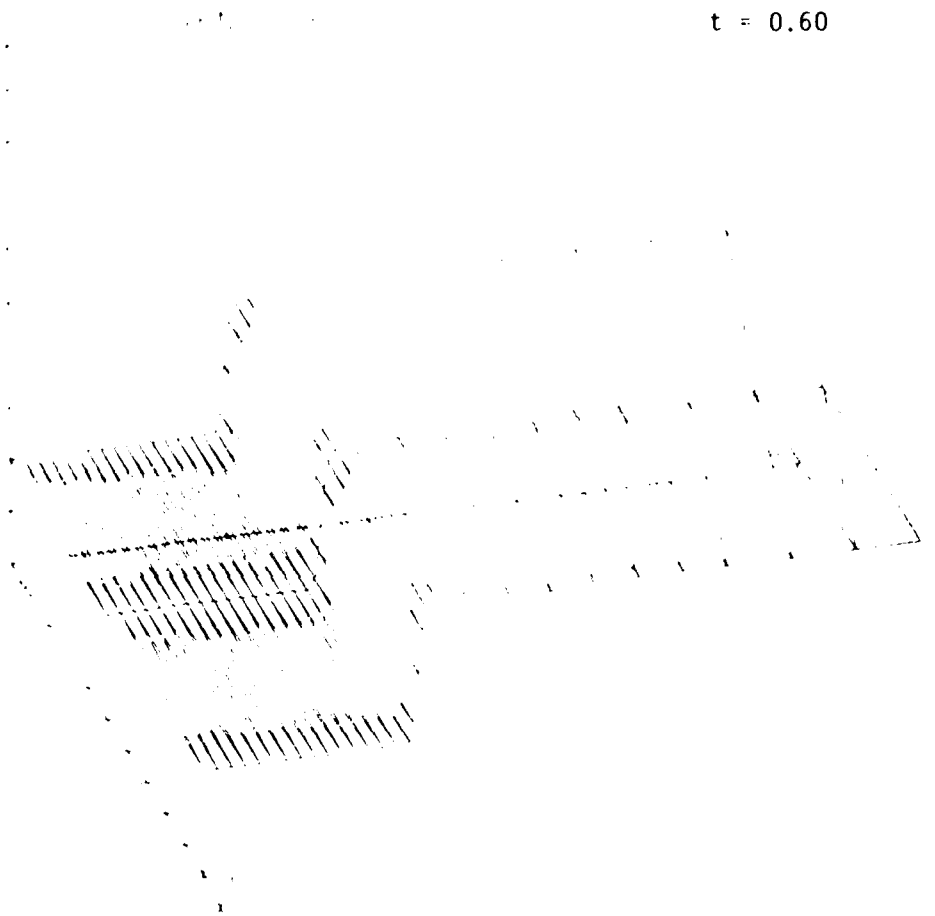

Figure 25. MFE Solutions of Laminar Navier-Stokes Equations for An Experimental Plane Shock of Deschambault and Glass Reflecting Against a Vertical Wall. (M_S = 2.05, Θ = 90°, p_t = 150 torr, ρ_t = 3.23 x 10^{-4} g/cm^3 in Argon). A 3 x 31 MFE Grid is Used.

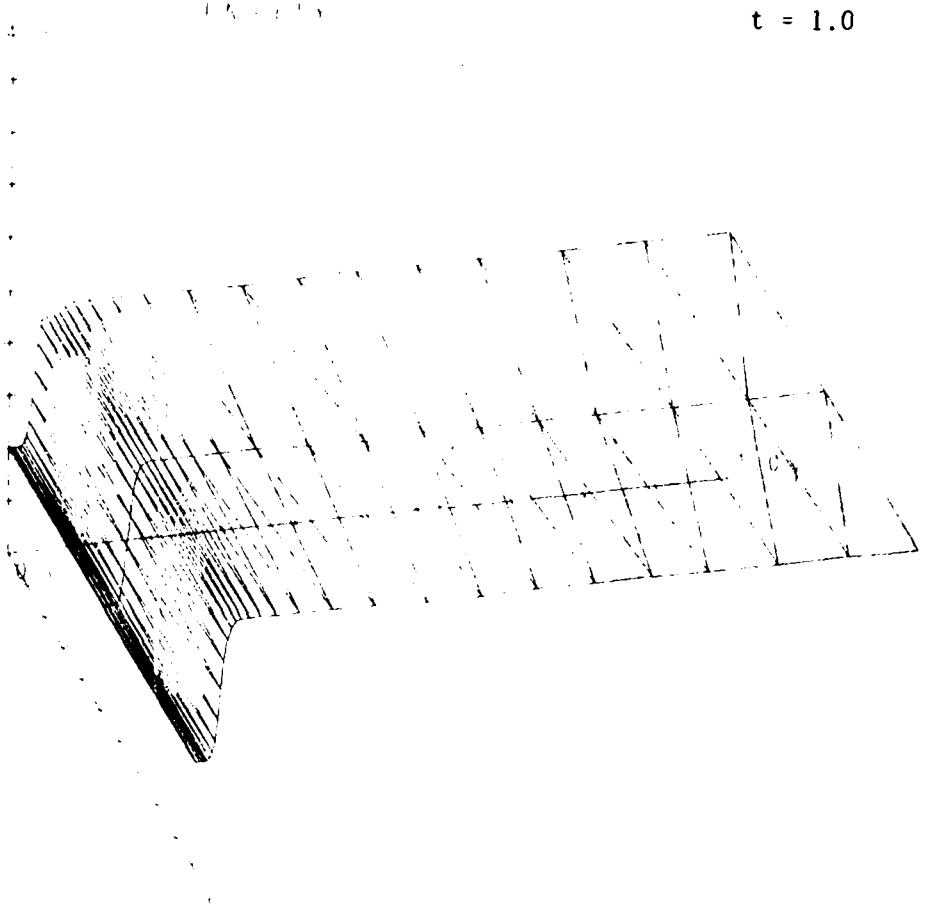

Figure 26. MFE Solutions of Laminar Navier-Stokes Equations for An Experimental Plane Shock of Deschambault and Glass Reflecting Against a Vertical Wall. (M_S = 2.05, Θ = 90°, p_+ = 150 torr, ρ_+ = 3.23 x 10^{-4} g/cm^3 in Argon). A 3 x 31 MFE Grid is Used.

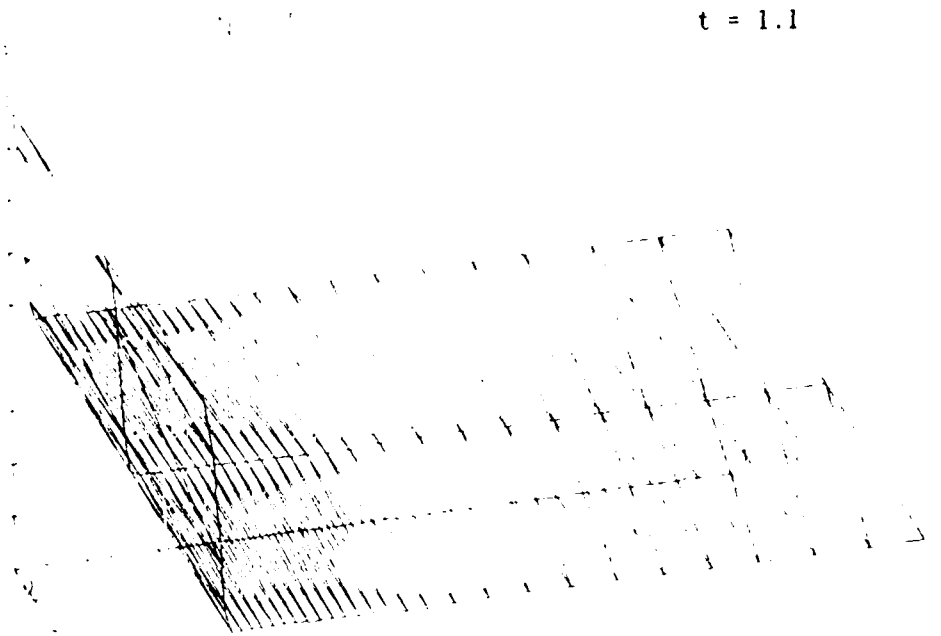

Figure 27. MFE Solutions of Laminar Navier-Stokes Equations for An Experimental Plane Shock of Deschambault and Glass Reflecting Against a Vertical Wall. (M_S = 2.05, Θ = 90°, p_+ = 150 torr, $\rho_+ = 3.23 \times 10^{-4} g/cm^3$ in Argon). A 3 x 31 MFE Grid is Used.

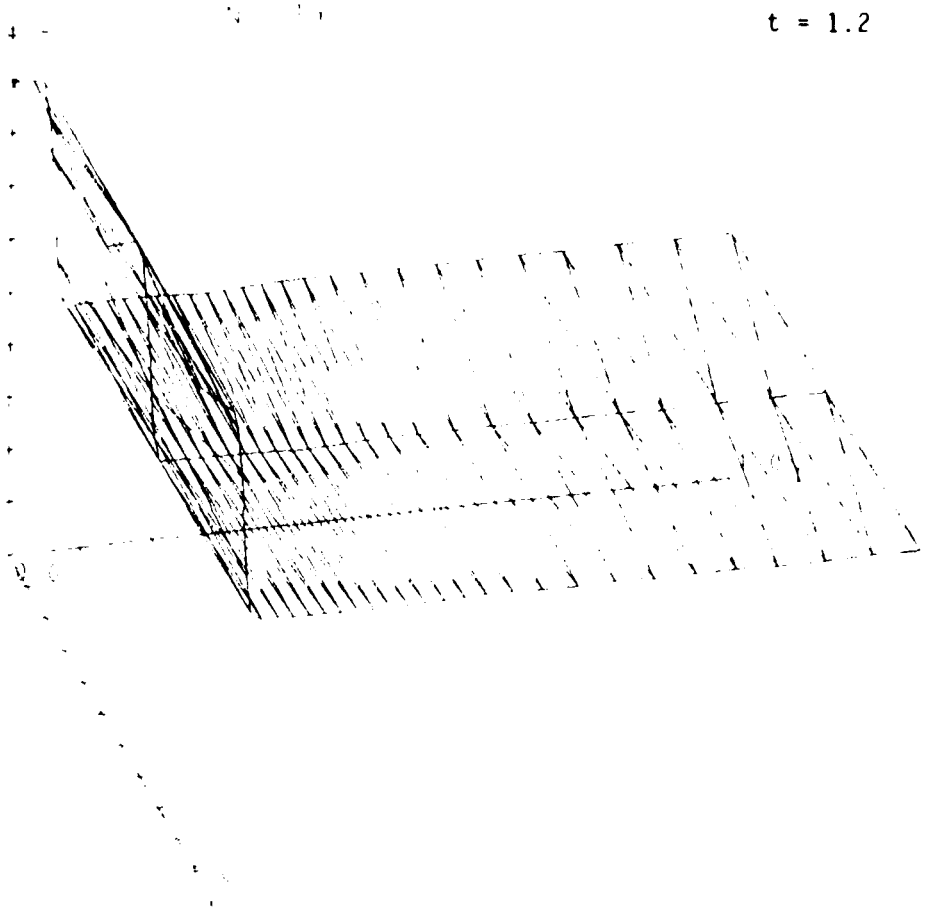

Figure 28. MFE Solutions of Laminar Navier-Stokes Equations for An Experimental Plane Shock of Deschambault and Glass Reflecting Against a Vertical Wall.
(M_S = 2.05, Θ = 90°, p_+ = 150 torr, ρ_+ = 3.23 x 10^{-4}g/cm^3 in Argon).
A 3 x 31 MFE Grid is Used.

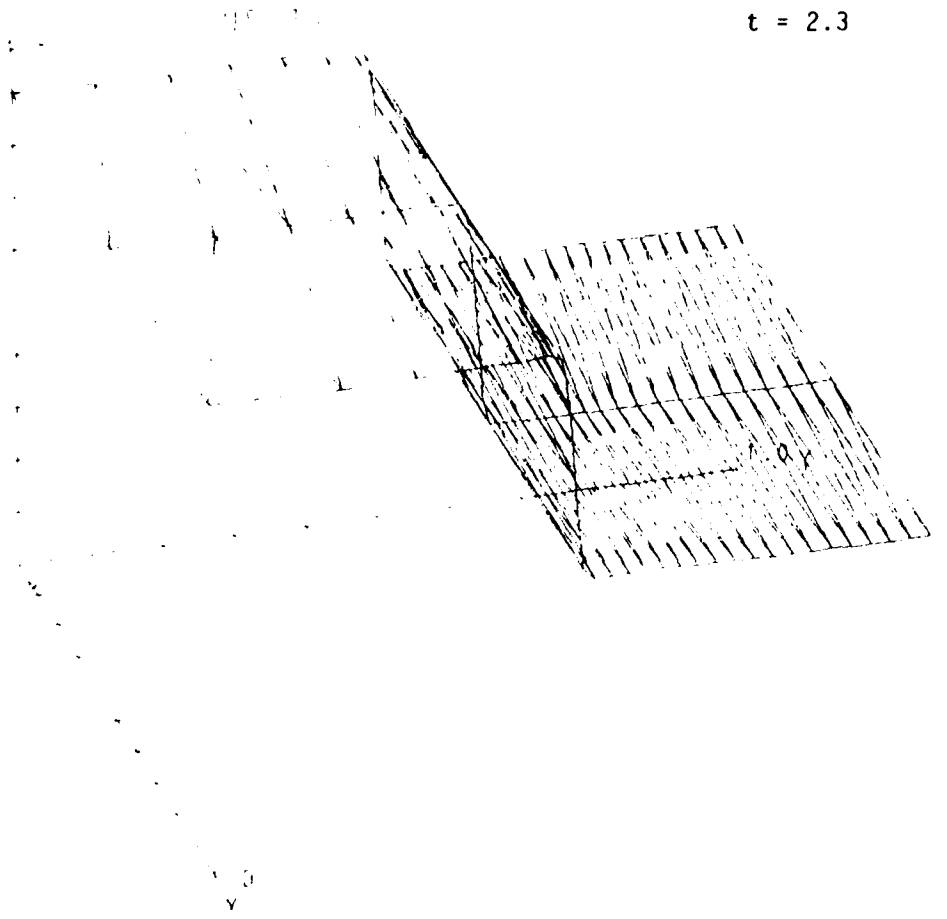

Figure 29. MFE Solutions of Laminar Navier-Stokes Equations for An Experimental Plane Shock of Deschambault and Glass Reflecting Against a Vertical Wall.
(M_S = 2.05, Θ = 90°, p_+ = 150 torr, ρ_+ = 3.23 x 10^{-4} g/cm^3 in Argon).
A 3 x 31 MFE Grid is Used.

t = 2.3

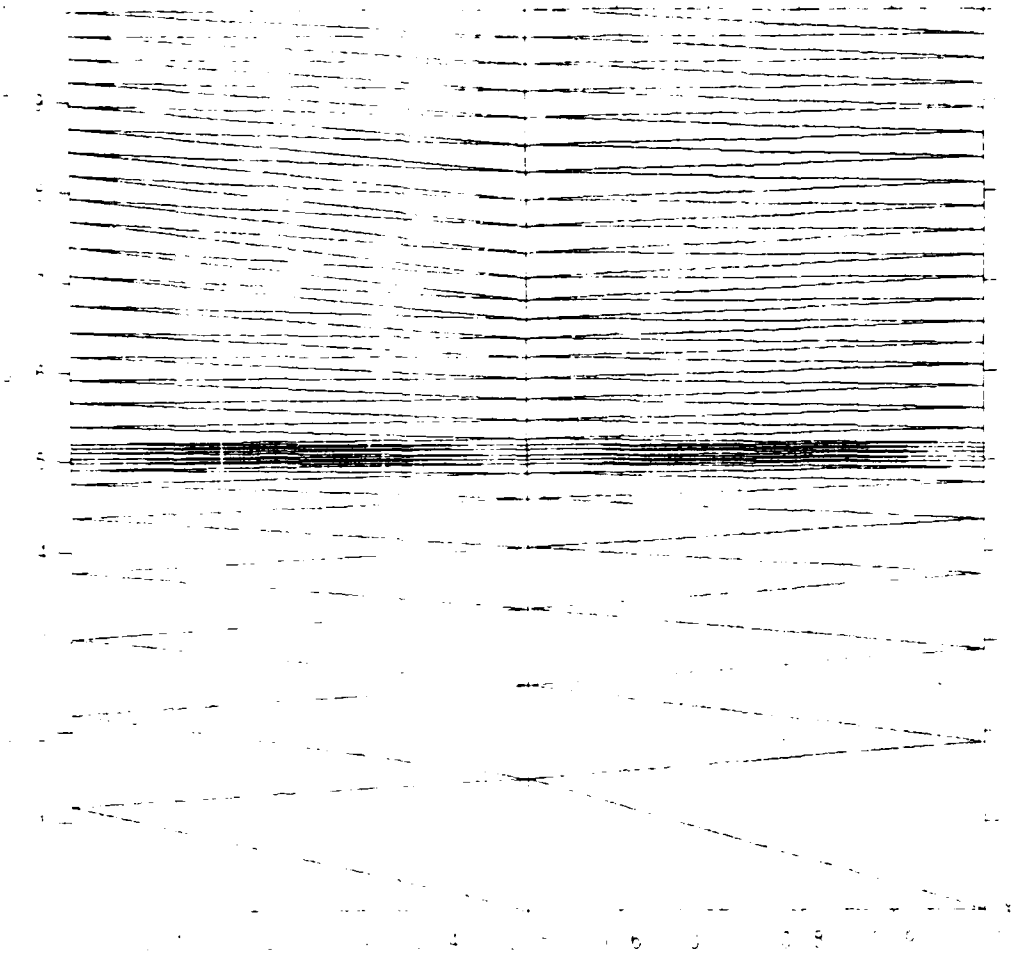

Figure 30. Projection of MFE Grid Mesh on the x-y Plane for an Experimental Plane Shock of Deschambault and Glass Reflecting Against a Vertical Wall. (M_s = 2.05, θ = 90°, p_+ = 150 torr, ρ_+ = 3.23 x 10^{-4} g/cm^3 in Argon). A 3 x 31 MFE Grid is Used.

with the macroscopic flow features. In this experimental example, it was undoubtedly the physics model which requires improvement more than the numerics. Because local turbulent dissipation rates exceed laminar rates by large factors, it is likely that this experiental example imposes more severe demands upon the PDE method than will be encountered in more realistic physical models of real shock environments (which have much larger-than-laminar dissipation rates).

In order to verify that the complex behavior in this example was truly associated with vorticity generation in the boundary layer, this same incident shock was propagated into, and reflected from, a vertical wall. Fluid shears do not occur in this example, and the MFE solutions appear in Figures 24 to 30. The shock profiles remain perfectly planar (to many significant figures) because only compressive and expansive forces act in this reflection process. Neither numerical dissipation nor anomalous vorticity effects were perceptible in these MFE solutions. It was also validated that the Rankine-Hugoniot and Taylor solutions of the steady reflected shock profiles were obtained in these solutions.

SECTION 3
CONCLUSIONS

The results of work during this phase of investigation continue to show promise for resolving shock-boundary layer interactions in 2-D according to PDE's which include the appropriate physical dissipation effects of airblast environments. The attempted resolution of a turbulent shock-boundary layer interaction problem using only laminar dissipation rates provided an unanticipated preview of physical modeling needs which may be required in high-resolution calculations when the numerical dissipation effects are successfully reduced to insignificant levels. In all cases, it presently appears in our MFE results that the highly local physical dissipation processes in regions of large fluid gradients can be sensitive determinates of macroscopic flow properties in shock-boundary layer interactions. The evolution of the physical dissipation effects over highly disparate scales in all of the MFE solutions computed to date exhibit remarkable levels of agreement with those corresponding descriptions which have appeared in the classic shock literature for real, viscous gases.

SECTION 4
RECOMMENDATIONS

This project has so far focussed on the feasibility of the MFE method contributing to the technology base for airblast studies. Accordingly, the work to date has revealed numerous research needs which should now be addressed in order to push onward toward real-world applications. These include:

1. Grid restructuring. The grid connections used in the existing MFE airblast code in 2-D contain certain biasing effects which would be undesirable in complex flow fields. Alternative grid connection schemes are available and should be developed for DNA applications.

2. Implement ADI methods of matrix solution for more efficient solution of problems on large grid meshes.

3. Extended benchmarking of MFE code against classic laminar flows. In the interest of feasibility projections, the testing of the current MFE code version has been applied to preview numerical requirements in some shock-boundary layer regimes which are well beyond the laminar Navier-Stokes model which is contained in this code version. It is now timely to drop back from this advanced stage of experimentation and systematically perform those numerous validations against some of the basic laminar boundary layer benchmark problems. Particular emphasis should be directed toward viewing the onset and development of both laminar and possible early turbulent flow transitions.

SECTION 5
LIST OF REFERENCES

1. Deschambault, R.L. and I.I. Glass, "An Update on Nonstationary Oblique Shock Wave Reflections: Actual Isopycnics and Numerical Experiments," Preprint, Institute for Aerospace Studies, University of Toronto, Toronto, Ontario, Canada, 1983.

2. Glass, I.I., presentation at Semi-Annual DNA Airblast Review Meeting, held at R&D Associates, Marina del Rey, CA, December 8-9, 1982.

DISTRIBUTION LIST

DEPARTMENT OF DEFENSE

DEFENSE INTELLIGENCE AGENCY
ATTN: RTS-2A (TECH LIB)
ATTN: RTS-2B

DEFENSE NUCLEAR AGENCY
ATTN: SPAS C GALLOWAY
ATTN: SPAS D MUNNINGHOFF
ATTN: SPAS G ULLRICH
ATTN: SPAS R ROHR
4 CYS ATTN: STTI-CA

DEFENSE TECHNICAL INFORMATION CENTER
12 CYS ATTN: DD

FIELD COMMAND DEFENSE NUCLEAR AGENCY
ATTN: FCTT
ATTN: FCTT W SUMMA
ATTN: FCTXE

JOINT STRAT TGT PLANNING STAFF
ATTN: JLKS
ATTN: JPTM
ATTN: JPTP

UNDER SECY OF DEF FOR RSCH & ENGRG
ATTN: STRAT & SPACE SYS(OS)
ATTN: STRAT & THEATER NUC FOR F VAJDA

DEPARTMENT OF THE ARMY

HARRY DIAMOND LABORATORIES
ATTN: SCHLD-NW-P
ATTN: SLCIS-IM-TL (81100) (TECH LIB)

U S ARMY BALLISTIC RESEARCH LAB
ATTN: SLCBR-SS-T (TECH LIB)

U S ARMY CORPS OF ENGINEERS
ATTN: DAEN-ECE-T

U S ARMY ENGINEER CTR & FT BELVOIR
ATTN: TECHNICAL LIBRARY

U S ARMY ENGINEER DIV HUNTSVILLE
ATTN: HNDED-SY

U S ARMY ENGR WATERWAYS EXPER STATION
ATTN: E JACKSON, WESSS-O
ATTN: J JACKSON, WESSD
ATTN: J ZELASKO, WESSD-R

U S ARMY NUCLEAR & CHEMICAL AGENCY
ATTN: LIBRARY
ATTN: MONA-NU MR LONG

U S ARMY STRATEGIC DEFENSE CMD
ATTN: DASD-H-SAV R C WEBB

U S ARMY STRATEGIC DEFENSE COMMAND
ATTN: ATC-T

DEPARTMENT OF THE NAVY

NAVAL RESEARCH LABORATORY
ATTN: CODE 2627 (TECH LIB)
ATTN: CODE 4040 D BOOK
ATTN: CODE 4040 J BORIS

NAVAL SURFACE WEAPONS CENTER
ATTN: CODE R44 H GLAZ
ATTN: CODE X211 (TECH LIB)

NAVAL SURFACE WEAPONS CENTER
ATTN: TECH LIBRARY & INFO SVCS BR

DEPARTMENT OF THE AIR FORCE

AIR FORCE CTR FOR STUDIES & ANALYSIS
ATTN: AFCSA/SAMI (R GRIFFIN)

AIR FORCE INSTITUTE OF TECHNOLOGY/EN
ATTN: LIBRARY/AFIT/LDEE

AIR FORCE WEAPONS LABORATORY, AFSC
ATTN: NTED-A
ATTN: SUL

BALLISTIC MISSILE OFFICE/DAA
ATTN: ENSN
ATTN: MYED D GAGE

STRATEGIC AIR COMMAND/NRI-STINFO
ATTN: NRI/STINFO

DEPARTMENT OF ENERGY

LOS ALAMOS NATIONAL LABORATORY
ATTN: C F KELLER
ATTN: M T SANDFORD
ATTN: R WHITAKER

SANDIA NATIONAL LABORATORIES
ATTN: DIV 7111 J W REED
ATTN: J R BANNISTER 7111
ATTN: ORG 7112 A CHABAI

OTHER GOVERNMENT

CENTRAL INTELLIGENCE AGENCY
ATTN: OSWR/NED

DEPARTMENT OF DEFENSE CONTRACTORS

ACUREX CORP
ATTN: C WOLF

AEROSPACE CORP
ATTN: H MIRELS
ATTN: LIBRARY ACQUISITION M1/199

APPLIED RESEARCH ASSOCIATES, INC
ATTN: N HIGGINS

APPLIED RESEARCH ASSOCIATES, INC
ATTN: D PIEPENBURG

BOEING CO
ATTN: S STRACK

CALIFORNIA RESEARCH & TECHNOLOGY, INC
ATTN: K KREYENHAGEN
ATTN: LIBRARY

CALIFORNIA RESEARCH & TECHNOLOGY, INC
ATTN: F SAUER

CARPENTER RESEARCH CORP
ATTN: H J CARPENTER

DENVER, UNIVERSITY OF
ATTN: J WISOTSKI

G B LABORATORY, INC
ATTN: G BURGHART

H & H CONSULTANTS, INC
ATTN: J HALTIWANGER
ATTN: W HALL

H-TECH LABS, INC
ATTN: B HARTENBAUM

KAMAN SCIENCES CORP
ATTN: R RUETENIK

KAMAN TEMPO
ATTN: DASIAC

KAMAN TEMPO
ATTN: DASIAC

MCDONNELL DOUGLAS CORP
ATTN: H HERDMAN
ATTN: R HALPRIN

MISSION RESEARCH CORP
ATTN: C LONGMIRE

NEW MEXICO, UNIVERSITY OF
ATTN: J KOVARNA

NICHOLS RESEARCH CORP, INC
ATTN: R BYRN

PACIFIC-SIERRA RESEARCH CORP
ATTN: H BRODE, CHAIRMAN SAGE

PACIFIC-SIERRA RESEARCH CORP
ATTN: D GORMLEY

PACIFICA TECHNOLOGY
ATTN: R ALLEN
ATTN: TECH LIBRARY

PATEL ENTERPRISES, INC
ATTN: M PATEL

PHYSICAL RESEARCH, INC
ATTN: R DELIBERIS
ATTN: W MENDES

PHYSICS INTERNATIONAL CO
ATTN: H W WAMPLER

R & D ASSOCIATES
ATTN: A KUHL
ATTN: T MAZZOLA
ATTN: TECHNICAL INFORMATION CENTER

R & D ASSOCIATES
ATTN: A POLK
ATTN: B WEBSTER

R & D ASSOCIATES
ATTN: G GANONG

RAND CORP
ATTN: B BENNETT

S-CUBED
ATTN: B PYATT
ATTN: C DISMUKES
ATTN: J BARTHEL
ATTN: LIBRARY

S-CUBED
ATTN: C NEEDHAM

SCIENCE & ENGRG ASSOC, INC
ATTN: B CHAMBERS

SCIENCE APPLICATIONS INTL CORP
2 CYS ATTN: R GELINAS

SCIENCE APPLICATIONS INTL CORP
ATTN: H WILSON
ATTN: R SCHLAUG
ATTN: TECHNICAL LIBRARY

DEPT OF DEFENSE CONTRACTORS (CONTINUED)

SCIENCE APPLICATIONS INTL CORP
ATTN: J COCKAYNE
ATTN: W LAYSON

SCIENCE APPLICATIONS INTL CORP
ATTN: G BINNINGER

SRI INTERNATIONAL
ATTN: J COLTON

TELEDYNE BROWN ENGINEERING
ATTN: D ORMOND
ATTN: F LEOPARD

TRW ELECTRONICS & DEFENSE SECTOR
ATTN A ZIMMERMAN
ATTN: M SEIZEW
ATTN: TECH INFO CTR,DOC ACQ

TRW ELECTRONICS & DEFENSE SECTOR
ATTN: E WONG, BLDG SB1
ATTN G HULCHER
ATTN: N GUILES
ATTN: N LIPNER
ATTN: P DAI

WEIDLINGER ASSOC, CONSULTING ENGRG
ATTN: I SANDLER

END

3-87

DTIC